Acta Geochim
https://doi.org/10.1007/s11631-021-00522-x

ORIGINAL ARTICLE

Early planetary processes and light elements in iron-dominated cores

Chaojia Lv[1] · **Jin Liu**[1,2]

Received: 20 July 2021 / Revised: 21 November 2021 / Accepted: 28 November 2021

Abstract This paper discusses the latest research on the accretion and differentiation of terrestrial planets and multidisciplinary constraints on light elements in iron-dominated metallic cores. The classic four-stage model of terrestrial planet formation advocates slow and local accretion. Meanwhile, the pebble accretion model suggests fast accretion for planets, while the Grand Tack model provides heterogeneous accretion mechanisms. Terrestrial planets and small interstellar bodies may have experienced at least some degree of partial melting due to the three primary energy sources (i.e., the decay of short-lived radioactive nuclides, the kinetic energy delivered by impacts, and the conversion of gravitational potential energy). Together with metal-silicate separation mechanisms, the magma ocean theory depicts the pattern of core formation in terrestrial planets. Several hypotheses have been proposed to explain the concentration of siderophile elements in the mantle, including the single-stage, continuous, and multistage core formation models, and the late-veneer model. Some light elements have been postulated in the core to account for Earth's outer core density deficit. A plethora of constraints on the species and concentration of light elements have been put forward from the perspectives of cosmochemical and geochemical fingerprints, geophysical observations, mineral physics, numerical modeling, and theoretical prediction. Si and O may be the two leading candidates for Earth's outer core light elements; however, it still remains an open question. S is another potential light element in Earth's core, most likely with less than 2 wt%. Other light elements including H and C, may not exceed 1 wt% in the core. Moreover, the accretion and differentiation history would provide some clues to light elements in other terrestrial planetary cores. In principle, a larger heliocentric distance corresponds to accretion from more oxidized materials, leading to a higher S concentration in the Martian core. On the contrary, Mercury is close to the Sun and has accreted from more reduced materials, resulting in more Si in the core.

keywords Terrestrial accretion · Early processes · Core-mantle differentiation · Core composition

1 Introduction

As one of the most important events in the early history of terrestrial planets, core formation involving a large degree or perhaps global melting of accreted substances has been widely concerned over the last few decades. Ringwood (1979) proposed that Earth formed from homogeneous materials and then went through internal differentiation before forming the metallic core and silicate mantle. Later, the magma ocean theory described the core formation scenarios for terrestrial planets and asteroids following the understanding of heating from short-lived radioactive elements (mainly ^{26}Al) and kinetic energy from impacts (Carlson et al. 2014). All the terrestrial planets and some asteroids in the Solar System show differentiation of the metallic core and silicate mantle. However, the core-forming conditions for individual planetary bodies differ

✉ Jin Liu
jin.liu@hpstar.ac.cn

[1] Center for High Pressure Science and Technology Advanced Research, Beijing 100094, China

[2] CAS Center for Excellence in Deep Earth Science, Guangzhou 510640, China

Published online: 21 January 2022

due to the variety of accretion rates, accreted materials, and planet sizes. For instance, the ratio of a planet and its core for Mercury is much smaller than that for Mars, mainly reflecting the chemical difference between their precursors during planetary accretion. Thus, the core formation event is vitally important for the geophysical and geochemical properties of the planets. Geochemical signatures, in turn, help constrain the accretion and differentiation history of planets.

Along with the core-mantle differentiation, the extent of elements partitioned into the metallic core depends on their siderophile nature at high pressure and temperature (*P–T*) conditions. Light elements including Si, O, S, C, and H have attracted considerable attention because of the core density deficit between the seismic model and pure iron at the outer core *P–T* conditions. The identity and abundance of light elements in the core have been extensively assessed in the light of geophysical observation, cosmochemical and isotopic studies, and high *P–T* experiments in the last few decades (Terasaki and Fischer 2016; Trønnes et al. 2019 and references therein). However, there are still many uncertainties around the composition and evolution of terrestrial planetary cores. High *P–T* experiments on iron-rich alloys often lead to inconsistent results while crucial measurements on terrestrial planets are scarce. Meanwhile, cosmochemical and isotopic data of meteorites present evidence of the origin and evolution history of terrestrial planets, which in turn, help pin down the potential light elements in iron-dominated metallic cores.

This review provides a synthesis of the current understanding of terrestrial planets' accretion and core-mantle fractionation scenes. The possible light elements in the Earth's core are examined in detail with constraints from cosmochemistry and isotopic fingerprints, high *P–T* metal-silicate partitioning experiments, and geophysical observations. The candidate light elements in the cores of other planetary bodies are also discussed.

2 Core formation scenarios

2.1 Terrestrial planet formation models

2.1.1 The classical model

Planet formation may have undergone four stages: dust sedimentation and growth, planetesimal growth, planetary embryo growth, and planet growth (including the giant impact) (Fig. 1). These stages likely took place simultaneously at different orbital radii in the solar disk, where the temperature, density, viscosity, and orbital period changed with the semi-major axis.

(1) Planet formation started in the nebular disk from a collapsing molecular cloud. Pre-existing dust would condensate from gas settling towards the mid-plane of the protoplanetary disk (Weidenschilling 1980). A balance could be realized between the turbulent diffusion of solid material and gravity, and a vertical equilibrium structure was assembled in the disk (Cuzzi et al. 1993; Dubrulle et al. 1995). Dust grains could grow via collisions in this structure. Detailed mechanisms for the accreting period can be found in Dominik et al. (2007) and Morbidelli and Raymond (2016).

(2) There are the 'radial drift' and 'bouncing' barriers during the accretion of planetesimals from dusts. A headwind causes the radial drift barrier at the boulders of Keplerian speeds, leading to energy loss and a spiral of orbits into the Sun (Whipple 1972). The bouncing barrier is the reducing efficiency of binary collisions due to colliding boulders bouncing or even fragmenting (Blum and Wurm 2008; Zsom et al. 2010). It is possible to grow large planetesimals via binary collisions if ice enhances stickiness and collision velocities remain below $\sim$ 50 m/s (Wada et al. 2009, 2013; Okuzumi et al. 2012). However, little is known about whether the formation of terrestrial planets in the Solar System could satisfy such strict conditions. In the following sections, the pebble model provides a more robust mechanism for forming planetesimals and embryos from nebular dusts.

(3) Once objects grew beyond the boulder barrier of planetesimals, the growth rate would depend on their sizes. Small planetesimals accreted slowly and alone in their physical cross-section. If planetesimals grew large enough, the escape velocities from their surfaces were greater than their relative velocities, and then gravitational focusing became important (Greenberg et al. 1978). The dynamical friction reduced the relative velocities of larger bodies compared to the rest. The larger bodies had wider collision cross-sections and hence grew faster into planetary embryos. Once the eccentricities reached orbit-crossing values, the planetesimals eventually collided. In other words, planetesimal growth changed into the 'runaway' process (Wetherill and Stewart 1989; Kokubo and Ida 1996). The dynamical fraction reduced the eccentricities and inclinations of larger bodies, while small bodies tended to fragment during a collision due to their higher relative velocities and lower gravitational binding energies. The runaway growth produced a bimodal mass distribution among the aggregation of planetesimals and planetary embryos. The growth of planetary

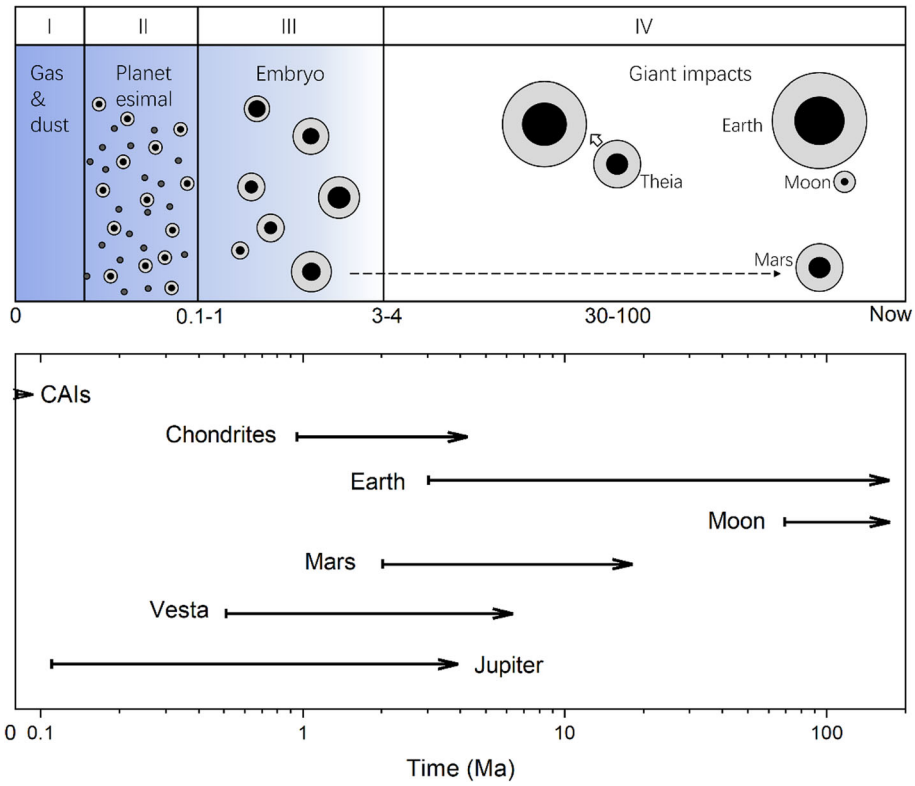

Fig. 1 Terrestrial planet formation stages and timescale. The upper panel is the illustration of terrestrial planets. The four stages are divided as follows: (I) dust settling, (II) planetesimal formation, (III) planetary embryo formation, and (IV) Giant impacts including the Moon-forming event. The formation scene corresponds to a two-stage accretion scenario (Yu and Jacobsen 2011). The shaded area represents the protoplanetary nebula in the Solar System before its extinction at $\sim$ 4 Ma (Bollard et al. 2017). The lower panel shows the accretion time. The formation of CAIs constrains the start point. The bottom of the arrow is constrained by the core formation for terrestrial planets, while the tip of the arrow indicates the crust formation or the end of accretion. The datasets of the accretion timescale are compiled from previous studies (McCubbin and Barnes 2019; Lammer et al. 2020a; Mezger et al. 2020)

embryos would be self-limiting, and the runaway formation slowed down due to viscous stirring (Lissauer 1987; Ida and Makino 1993). The growth changed into the 'oligarchic' stage, wherein the bimodal mass distribution remained. Approximately half of the solid mass was in the embryos, while the other half was in planetesimals in the accretion disk. Orbital repulsion caused planetary embryos to part from each other at about 10 mutual Hill radii (Kokubo and Ida 1995).

(4) The oligarchic growth ended once the dynamical friction could not maintain the orbits of planetary embryos. It occurred when the number of planetesimals was substantially depleted. If the gas drag, instead of planetesimals, was the main source of dissipation, then removing nebular gas resulted in the termination of the oligarchic growth (Iwasaki et al. 2002; Zhou et al. 2007). Once the gravitational stirring between large bodies overcame the dissipation force from gas disk and/or planetesimals, planetary embryos perturbed each other onto crossing orbits, resulting in giant impacts or scattering events (Wetherill 1985). In the following impact events over tens of millions of years, the embryos had stable orbits, and the planets finally formed.

2.1.2 *The fast accretion and the pebble model*

The accretion scenarios of dust growth, runaway growth, and oligarchic growth were too slow compared with removing nebular gas and forming Mars (a planetary embryo) (Levison et al. 2010). Besides, it is hard to explain the 10–100 km-sized objects in the asteroid belt based on the bimodal accretion in the classical model. In the past decade, the pebble (millimeter to decimeter) accretion was proposed to form large planetesimals and planetary embryos directly from dusts. Notably, the Roche density, at which point the particles would no longer be pulled apart by the gravity of the Sun, was hard to surpass for small particles due to the sediment turbulence (Weidenschilling 1995). Youdin and Goodman (2005) provided the 'streaming instability' process to robustly concentrate pebbles beyond the Roche density. In this process, the

pebbles formed clumps. Since pebbles moved faster than clumps, the clumps continued growing up until a point at which they gravitationally collapsed and formed planetesimals. However, it is debated whether planetesimals could form generically in a nebular disk (Hughes and Armitage 2012; Krijt et al. 2016).

Other pioneering work suggested that pebbles might be captured in small, turbulent eddies if the disk was turbulent (Cuzzi et al. 2008). The eddies pushed particles to the outer edges and condensed particles to exceed the Roche density. A local high-pressure area in the disk, either caused by a zonal flow (Johansen et al. 2009; Simon and Armitage 2014) or viscosity change within the disk (Kretke and Lin 2007; Lyra et al. 2008), could result in the formation of pebbles. The inward movement of icy pebbles at the snow line caused a pile-up of silicate grains, which could also lead to the formation of planetesimals (Ida and Lin 2008; Ida et al. 2016).

At the later accretion stage of planetesimals, they were likely embedded within a sea of pebbles. The pebbles would continue moving inwards because of the pressure gradient in the disk. Once the pebbles passed planetesimals, they would be accreted efficiently by the latter since the capture cross-sections of pebbles were very large (Johansen and Lacerda 2010; Ormel and Klahr 2010). Similar conditions are also applicable to the accretion of planetary embryos. Pebble accretion was extremely rapid and essential to interpret the formation of planets (Lambrechts and Johansen 2012), explaining the rapid accretion of giant planets before the removal of gas in the disk. It also improves our understanding of the accretion of terrestrial planets. To date, the pebble accretion theory is still too young, and some details are still unclear. It requires more study to clarify the early accretion of planetesimals and embryos in the future.

2.1.3 The Grand Tack model

Classical models have been proposed to simulate the later formation stages of terrestrial planets. They set the outer boundary of the terrestrial disk by Jupiter, given that it is mainly unstable orbiting outside the inner 3:2 mean-motion resonance with Jupiter (Walsh and Levison 2016). However, these classical models, including (1) eccentric Jupiter and Saturn at current orbits, (2) extra-eccentric Jupiter and Saturn, and (3) circular Jupiter and Saturn pre-Nice 2.0 model, all failed to predict a small planet forming near 1.5 AU (referred to as Mars). A narrow over-packed disk with the outer border truncated at 1 AU ideally generated the small mass of Mars, but how to generate such a truncated protoplanetary disk is still unknown (Hansen 2009).

Walsh et al. (2011) came up with the Grand Tack model to solve the small Mars problem (Fig. 2). In the Grant Tack

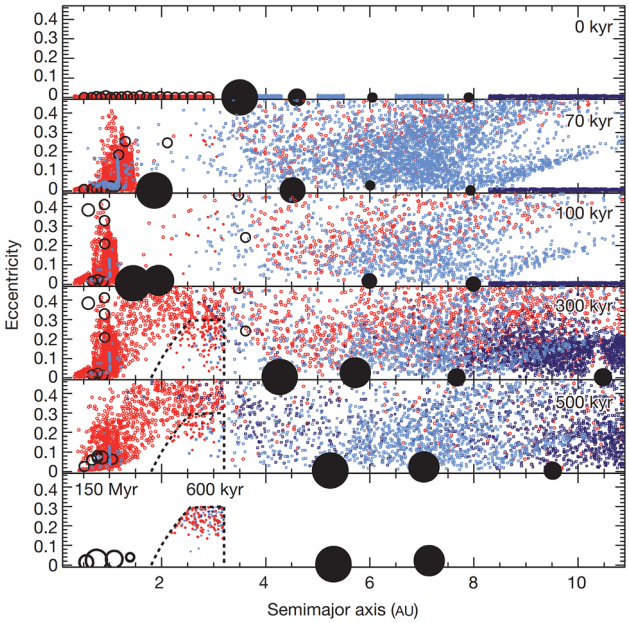

Fig. 2 An illustration of the Grand Tack model (Walsh et al. 2011). The filled black circles indicate Jupiter, Saturn, Uranus, and Neptune. The open black circles represent the planetary embryos (not in scale relative to the giant planets). The red, light blue, and dark blue dots represent volatile-poor planetesimals initially located between 0.3 and 3 AU, volatile-rich planetesimals between giant planets, and volatile-rich planetesimals initially located between 8 and 13 AU, respectively. For all planetesimals, the filled dots denote that they are inside the main asteroid belt, while the open dots are outside. The terrestrial planet pattern has been successfully simulated with the Grand Tack model. Copyright Walsh et al. (2011)

model, giant planets had a relatively short accretion timescale than terrestrial planets. As a result, Jupiter could carve an annular gap in the nebular disk and be pushed to migrate toward the Sun due to the imbalanced torques acting on the planet from the protoplanetary disk (Lin and Papaloizou 1986). Saturn also captured its gaseous envelope, although more slowly than Jupiter. Thus, Saturn would migrate very close to Jupiter, reaching an exterior 2:3 mean motion resonance with Jupiter (Masset and Snellgrove 2001). The particular configuration of the orbital spacing and mass ratio between Jupiter and Saturn reversed the total torque on the giant planets by protoplanetary gas, leading to the reverse of migration outwards.

The inward-then-outward migration of giant planets provides a viable mechanism to form a truncated disk for terrestrial planets. If Jupiter reversed its migration at 1.5 AU, the disk for terrestrial planets would truncate at 1 AU (Walsh et al. 2011). Almost all the protoplanets and planetesimals that originally formed beyond 1 AU were scattered outwards by Jupiter. This tack migration would lead to the high mass ratio between Earth and Mars, and the low amount of mass in the asteroid belt area. The Grand Tack model can further account for the semi-major axis

distribution of the terrestrial planets and the stirred demography of the asteroid belt (DeMeo and Carry 2014; Brasser et al. 2018).

In classical models, terrestrial planets mainly accreted locally. However, in the Grand Tack model, accretion was restricted to an annulus between ~ 0.5 and 1 AU, where materials from the outer part of the protoplanetary disk were also included. A total of 1–3 % mass for terrestrial planets were accreted from the outer planetesimals. The heterogeneous accretion materials may explain the similarity of the D/H ratio between carbonaceous chondrites and Earth's water (Walsh et al. 2011). The formation scene differs from previous classical models since Jupiter migrated across the asteroid belt twice in the Grand Tack model. The inward scattering of materials generated the asteroid belt during the outward migration of giant planets. Thus, materials in the asteroid belt came both the outer and inner Solar System, corresponding to the C type and S type asteroids.

2.2 Magma ocean theory and core formation

The magma ocean concept was raised after the petrological discovery from the Apollo program (Wood et al. 1970; Taylor and Jakeš 1974). Findings included the existence of a global, almost monomineralic anorthositic crust and the depletion of the mantle source of some mare basalts in Eu which is enriched in the lunar crust. Nowadays, the magma ocean theory has been adopted for terrestrial planets and asteroids.

2.2.1 Heat sources for magma ocean

The redistribution of silicate and metal from undifferentiated chondrites, known as the core formation process, needs deformation and fluxion. Since neither silicate nor metal is deformable at low temperatures, an elevated temperature is definitely needed. The heat mainly comes from the three sources as follows.

The first is the decay of short-lived radioisotopes. ^{26}Al is the most important short-lived radioisotope in the early Solar System because of its relatively high abundance and a short half-life of ~ 0.7 Ma (Gray and Compston 1974). ^{60}Fe with a half-life of ~ 2.6 Ma is the secondary radioisotope due to its relatively lower concentration (Tang and Dauphas 2012). The heat conduction timescale for a silicate sphere is quadratically proportional to the radius. Therefore, an asteroid with a diameter greater than 30 km accreted within the first million years could have be heated by ^{26}Al. However, due to the short half-life of ^{26}Al, only planetesimals or embryos that accreted within ~ 2 Ma after the first solids in the Solar System, could be molten in this way (Elkins-Tanton 2012).

The second heat source is the energy release of impactors. The kinetic energy of impact was largely converted into heat, while the depth of heating depended on the impactor size. If all the gravitational potential energy were converted to heat, the global temperature increment (ΔT) was given by $\Delta T \approx 35{,}000\ \mathrm{K}\ (M/M_E)^{2/3}$, where M and M_E are the mass of impactor and Earth, respectively (Rubie et al. 2015). Such a function is oversimplified; nevertheless, it provides a rough estimate that a Mars-sized (≈ 0.1 M_E) impactor would wholly melt the proto-Earth ($\Delta T \approx$ 7500 K). On the other hand, Canup (2008) suggested that a Moon-forming impact might have melted Earth to a depth of 2000 km. Tonks and Melosh (1993) argued that global melting would require a projectile to be at least 40% the mass of the Earth.

The third heat source is the release of gravitational potential energy during iron sinking towards the metallic core (Nimmo and Kleine 2015). This heat source was relatively weak but deposited locally, which would reduce local viscosities (Ricard et al. 2009; Šrámek et al. 2010). Based on Canup (2008) and references therein, the ΔT for terrestrial planets would be 10^3–10^4 K if all accretionary energy was instantaneously applied to the whole planet. Therefore, the sources above nearly comprised the total heating budget during planetary accretion and differentiation. Notably, the heat was not delivered to planets all at once or homogeneously. As a matter of fact, the discrete intervals of heat added to the growing planets could result in multistage melting and metal-silicate segregations over their accretion timescale from planetesimals to planetary embryos and then to planets.

2.2.2 Core segregation mechanisms

Terrestrial core formation involved iron-rich metal segregating from the mantle. If the bulk silicate Earth (BSE) was not globally molten, liquid iron could travel through the solid mantle via grain-scale percolation, the descent of kilometer-size diapirs, and/or fracture in the solid mantle (Fig. 3). On the other hand, if the temperatures were high enough to melt silicates entirely, a global-scale magma ocean would form, and iron liquid could descend efficiently and rapidly to the core (Stevenson and Scott 1991; Rubie et al. 2003). Furthermore, chemical equilibrium between the silicate mantle and metallic core could occur during core-mantle separation. However, due to the slow diffusion rates in crystalline silicates and the large scales of metals and silicates, the diapir and fracture mechanisms are inefficient to reach chemical equilibration (Rubie et al. 2011, 2015). Here, we discuss the chemical equilibration in the grain-scale percolation and global magma oceans through giant impacts.

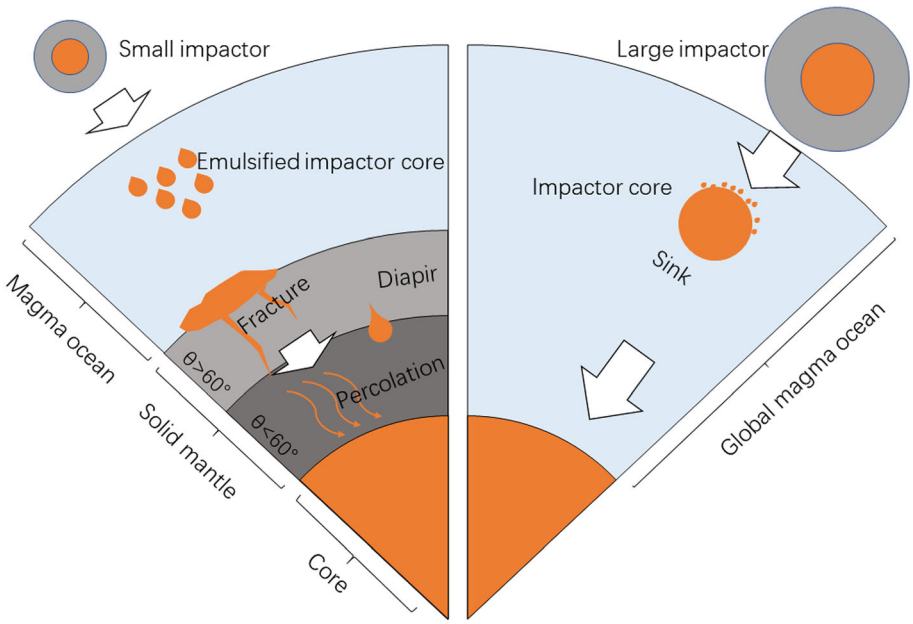

Fig. 3 Metal segregation mechanisms. Left panel: the situation with small impactors (the low-temperature scenario). Only part of the mantle is molten at the surface. Iron accumulates at the bottom of the magma ocean and forms molten metal ponds. Liquid iron passes through the solid mantle via large-scale fracture and diapir mechanisms and/or small-scale percolation if the dihedral angle is less than 60°. Right panel: the situation with large impactors (the high-temperature scenario). The whole mantle is molten. Whether the metal-silicate chemical equilibrium is reached depends on the size of droplets formed from the impactor's core

(1) *Grain-scale percolation* The dihedral angle is the key for percolation between two solid–liquid boundaries where they intersect a solid–solid boundary at a triple junction (Stevenson and Scott 1991; Rubie and Jacobson 2016). When the dihedral angle is less than 60°, liquid metal could be fully connected along grain boundaries and percolate efficiently through solid silicate matrices. Once the dihedral angle is higher than 60°, a small fraction of liquid metal would form isolated pockets. They would be connected when the metal fraction reaches a critical value of 2–6% for the dihedral angle range of 60°–85° (Walte et al. 2007). Experiments revealed that dihedral angles significantly exceeded 60° up to 25 GPa and were barely affected by pressure, temperature, and the species of solid phases (Rubie and Jacobson 2016). Notably, dihedral angles decreased with increasing concentrations of light elements, except Si and C (Terasaki et al. 2005). Other studies pointed out that dihedral angles decreased to 51° at 47 GPa and 23° at 64 GPa at 3000 K, but their experiments were likely subjected to high differential stress (Takafuji et al. 2004; Shi et al. 2013). Thus far, the efficiency and degree of chemical equilibration between silicate and core via percolation have never been modeled quantitatively.

(2) *Global magma ocean* The Moon-forming giant impacts involved collisions of planetary embryos with the proto-Earth. Such impacts produced substantial heat to melt the whole mantle to generate global magma oceans (Tonks and Melosh 1993; Rubie et al. 2015). The mantle-core segregation process was rapid and efficient in those scenes because of the conspicuous density contrast and very low viscosity of ultramafic silicate liquids under high pressure (Liebske et al. 2005). Most impactors likely underwent differentiation with a metallic core before reaching Earth. In some cases, the metallic cores of the impactors could remain intact and merge directly with the Earth's proto-core. However, impactors would often be emulsified partially or entirely into small droplets in magma oceans (Rubie et al. 2003). The metal-silicate interfacial energy controlled droplet size, and the stable droplet was typically ~ 1 cm in diameter with a settling velocity of ~ 0.5 m/s. Chemical equilibrium between the core and mantle would be very limited in the former but complete in the latter, respectively (Rubie et al. 2003).

2.2.3 *Earth's core formation models*

(1) *Single-stage core formation*. At the outset, metal-silicate segregation and core formation were thought to take place at a single set of *P–T-fO*$_2$ conditions (Li and Agee 1996; Gessmann and Rubie 2000; Wade and Wood 2005; Righter et al. 2011). A large *P–T* range of 25–60 GPa and 2200–4200 K was obtained with this model in which the *fO*$_2$ was generally fixed at two log units below the iron-wüstite buffer (IW-2). The precondition of this hypothesis is that the *P–T* conditions of chemical equilibrium between the mantle and core correspond to the bottom of the magma ocean. This scenario appears a little bit

simple given the Earth's late-accretion history. Nevertheless, the single-stage core formation model is beneficial to establish an intuitive image of the *P–T* conditions for metal-silicate equilibrium during core formation.

(2) *Continuous core formation* In a more realistic picture of core formation, Earth accreted its mass gradually with the changing conditions of core formation. Wade and Wood (2005) proposed the continuous core formation model in which each batch of incoming planetesimals would equilibrate with magma oceans on Earth. The metal-silicate equilibration *P–T* conditions would increase during the growth of the core. Thus, oxygen fugacity should not be fixed. Otherwise, the abundance of siderophile elements in the mantle cannot be reproduced. Rubie et al. (2011) argued that the fO_2 increased by $\sim$ 2 log units during accretion. Consequently, the FeO content in the mantle would increase from less than 1 to 8 wt%. Three major mechanisms for elevating the mantle oxidation state have been proposed. First, Si partitions into the core, which leads to the increase of FeO content in the mantle by the reaction:

$$\underset{\text{core mantle}}{2\text{Fe} + \text{SiO}_2} \rightarrow \underset{\text{mantle core}}{2\text{FeO} + \text{Si}} \quad (1)$$

Second, accreted materials become more oxidized during the later stages of accretion. The third mechanism is the disproportionation of ferrous iron in the mantle (Wade and Wood 2005). Alternatively, core formation might occur under relatively oxidizing conditions (Rubie et al. 2004; Siebert et al. 2013). In this model, the initial FeO content was $\sim$ 20 wt% in the mantle. Thus, a large amount of FeO could have been partitioned into the core during the accretion to reach the current FeO value of 8 wt% in the mantle. However, if a small amount of Si is also partitioned into the core, this model would fail based on the mass balance (Siebert et al. 2013; Rubie et al. 2015).

(3) *Multistage core formation*. The preliminary multistage model is based on an idealized accretion scenario in which Earth accreted through collision with different impactors that had $\sim$ 10 % of the Earth's mass (Rubie et al. 2011). Compared with the previous models, the bulk compositions of accreting bodies were determined in terms of their nonvolatile elements, while the oxygen content was the main compositional variable. Only a highly reduced composition and a relatively oxidized composition were adopted for simplification. The best fit indicates that Earth initially accreted from reduced materials by 60–70 % and then from more oxidized materials by 30–40 %.

The multistage core formation model has been significantly improved with N-body accretion simulations and the Grand Tack accretion model (Walsh et al. 2011; Rubie et al. 2015). The accreted materials are classified based on the heliocentric distance. The simulations indicate that metal-silicate equilibration pressures are, on average, 60–70 % of core-mantle boundary pressures at the time of each impact. Meanwhile, a large fraction of the impactors' iron core (70–100 %) could equilibrate with the silicate portion of protoplanets during each core formation event. The model also brings constraints on the light elements in the Fe-rich cores. 8–9 wt% Si, 2–4 wt% O, and 10–60 ppm H were suggested for the Earth, whereas less than 1 wt% Si and O for Mars (Rubie et al. 2015).

2.2.4 *Chronometer and timescale of terrestrial accretion/core formation*

Over the years, the formation of the Solar System has been explained by many different models. In general, timing is an essential factor in understanding the beginning of the Solar System, the rate of accretion, and the age of planet formation. Thus far, a good number of short-lived isotopes have been employed as the chronometer of core formation, such as ^{182}Hf–^{182}W, U–Pb (Harper Jr and Jacobsen 1996; Yin et al. 2002; Halliday 2004; Jacobsen et al. 2008; Kleine and Walker 2017), ^{50}Ti, ^{54}Cr, ^{92}Mo, ^{100}Ru (Dauphas 2017; Brasser et al. 2018; Carlson et al. 2018; Woo et al. 2018), ^{48}Ca/ ^{44}Ca (Schiller et al. 2018), atmospheric ^{36}Ar/ ^{38}Cr, ^{20}Ne/ ^{22}Ne (Marty 2012; Lammer et al. 2020b), ^{3}He abundance in the mantle, and D/H in Earth's sea water (Lammer et al. 2020b).

Hf-W is one of the most useful chronometers to determine the time of core formation. A brief review of its principle is provided here (Jacobsen 2005; Kleine et al. 2009). The now-extinct radionuclide ^{182}Hf decayed to ^{182}W with a half-life ($t_{1/2}$) of 8.9 Ma, comparable to the timescale of terrestrial planet formation. Both Hf and W are refractory; therefore, little Hf-W fractionation was in the nebula gas and dust. However, core-mantle segregation resulted in substantial Hf-W fractionation since lithophile Hf strongly partitions into silicate mantle, while W is moderately siderophile preferentially entering the metallic core. Thus, for core formation before the extinction of ^{182}Hf (several times of its half-life), the mantle would have excess ^{182}W. On the other hand, for core formation after the extinction of ^{182}Hf, there would be no endogenetic ^{182}W in the mantle. Therefore, the abundance of ^{182}W in the mantle can be adopted to determine the timing of the core formation. Note that the Hf/W chronometer depends

on several factors, including the initial Hf/W ratio in the bulk composition of the planets, the proportion of the core, and the degree of the metal-silicate partition (Righter and Shearer 2003).

The formation of the first solid grains in the Solar System (Ca-Al-rich inclusions, CAIs) has been defined as the beginning of the Solar System with an absolute age of 4,567.30 ± 0.16 Ma (Connelly et al. 2012). CAIs were largely considered to form in the hot inner protoplanetary disk, whereas some studies suggest CAIs formed in the outer Solar System (Warren 2011; Larsen et al. 2020). The growth of Mars was nearly completed when the nebula disk dissipated at 3.3–4.5 Ma following the formation of CAIs (Bollard et al. 2017; Wang et al. 2017). At the same time, Earth only accreted 0.5–0.6 of its total mass (M_E). Earth accreted most of its mass (> 0.8 M_E) within the first 10–30 Ma. The Moon-forming event brought Earth's main phase of accretion to an end between 30 and 100 Ma (Jacobsen 2005; Halliday 2008; Barboni et al. 2017; Connelly et al. 2019).

3 Interdisciplinary constraints on terrestrial core composition

Earth's core constitutes about one third of the total mass M_E and its component is still under debate. Since no direct core specimen is available, our understanding of the Earth's core primarily depends on geochemical fingerprints and geophysical observations. Specifically, seismology, geodesy, paleomagnetism, and isotope geochemistry provide direct constraints on the structure and state of the core; and geochemistry, cosmochemistry, and meteoritics guide the identity and abundance of light elements in the core. Besides, high *P–T* experiments and ab initio calculations bring further constraints on the composition and evolution of the Earth's core.

3.1 Cosmochemical constraints

In this section, the Earth's core composition is discussed from a cosmochemical perspective. A four-step process is summarized by McDonough (2014) to build up cosmochemical estimates of core composition: (1) assess the composition of the BSE; (2) define a volatility curve for the planet based on the abundances of volatile lithophile elements in the BSE; (3) calculate the bulk composition of the Earth based on the volatility curve defined in step (2); and (4) estimate the core composition by subtracting the BSE composition from the composition of the bulk Earth. The compositional models of the BSE were generally derived from mantle xenoliths and cosmochemical data (McDonough and Sun 1995; Palme and O'Neil 2014). Assuming no lithophile elements exist in the iron-rich core, the volatile trend at ~1 AU from the Sun can be built from the negative correlation between the relative abundance of element and the log 50 % condensation temperature at 10^{-4} atm (Fig. 4). Then the composition of the bulk Earth can be derived based on the abundances of lithophile elements and iron partitioning between the mantle and core (McDonough 2001).

One core compositional model was established using the method by McDonough (2014) (Table 1). In addition to Fe and Ni (Fe/Ni = 16.5), several candidate light elements have been suggested to exist in the core (e.g., H, C, S, Si, P, O, and N). The total content of S, C, and P may only constitute a minor fraction (~ 2.5 wt%) of the core, which is not enough to account for the core density deficit of Earth's outer core (McDonough 2014). Si (6 wt%) or O (3 wt%) may be the most abundant light element in the core. Notably, the solubility of Si in the metallic iron melt are greatly affected by the existence of O and extreme *P–T* conditions (Li and Fei 2014; Hirose et al. 2017).

3.2 Metal-silicate partitioning

3.2.1 Chemical partitioning rules

Siderophile elements tended to migrate from the BSE to the metallic core, especially before the crystallization of magma oceans. The partition of an element *M* can be expressed in a simplified way:

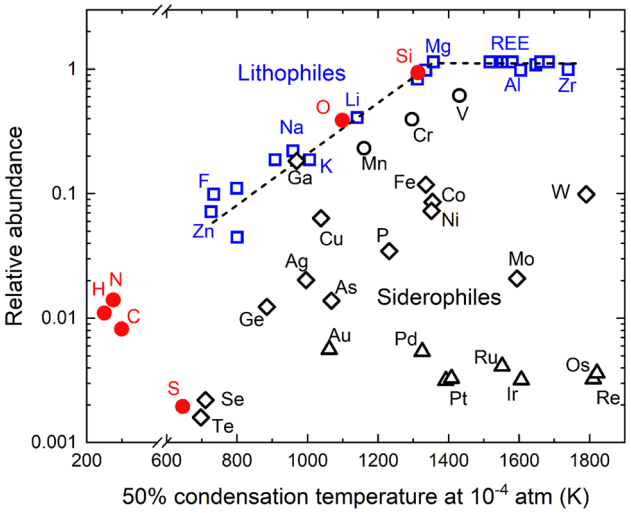

Fig. 4 Element abundance in the bulk silicate Earth (BSE) as a function of 50 % condensation temperature. The abundance in the BSE and those in the CI carbonaceous chondrites are normalized to $Mg_{BSE}/Mg_{CI} = 1$. The abundances of elements against the 50 % condensation temperature are from a gas of solar composition at the pressure of 10^{-4} bar. The depletion of elements in the BSE could be attributed to volatilization and chemical partitioning between silicate and metal. Modified from McDonough (2014)

Table 1 Candidate light elements in Earth's outer core

	O	Si	S	C	H	N	
Geochemical constraints	4	7.3	2.3				Allègre et al. (1995)
	0	6	1.9	0.2	0.06		McDonough (2014)[a]
	3	0	1.9	0.2	0.06		McDonough (2014)[a]
	< 1	4–5	1.9	0.2	0.1		Wood et al. (2006)
Metal-silicate partitioning	0.5	8	2				Rubie et al. (2011)
	4.5–5.5	1.5–2.2					Siebert et al. (2013)
	5.1–6.6	2.1–2.6					Fischer et al. (2015)
	1	2–4		0.15	0.035	0.003	Zhang and Yin (2012)
			1–1.2				Suer et al. (2017)
					0.3–0.6		Tagawa et al. (2021)
				0.09–0.2			Fischer et al. (2020)
						< 0.01	Speelmanns et al. (2019)
Mineral physics	0.5		9.5				Huang et al. (2011)
		10					Zhang et al. (2014)
	3.7	1.9	0	0			Badro et al. (2014)
	2.7–5	2–3.6					Badro et al. (2015)
	0.5–1	5–6	1.8–1.9	2			Litasov and Shatskiy (2016)
		1.6		0.7			Li et al. (2018)
	2.7		2.2	1.0			Yokoo et al. (2019)
	8.2		0.7	2.0			Yokoo et al. (2019)

All the values are in the unit of wt%

[a]Two alternative compositions were provides in one research

$$MO_{n/2}^{silicate} = M^{metal} + \frac{n}{4}O_2^{gas} \quad (2)$$

where n is the valence of ion M in the silicate. The distribution of elements between the metallic core and the BSE can be expressed as partition coefficients:

$$D_M^{metal-silicate} = X_M^{metal}/X_M^{silicate} \quad (3)$$

where X_M^{metal} and $X_M^{silicate}$ are the concentration of M in metal and silicate (in wt% or molar ratio), respectively. Once the concentration of a specific element in the BSE and its partition coefficient at the metal-silicate equilibrium conditions are ascertained, one could derive the light element concentration in the core.

Oxygen fugacity is an important factor of the partition coefficient, as shown in reaction (2). To separate the partition coefficient from oxygen fugacity, one can normalize the partition of element M to iron in the form of an exchange reaction (Wade and Wood 2005):

$$MO_{n/2}^{silicate} + \frac{n}{2}Fe^{metal} = FeO^{silicate} + M^{metal} \quad (4)$$

The distribution coefficient K_D is defined as:

$$K_D = \frac{D_M^{metal-silicate}}{(D_{Fe}^{metal-silicate})^{n/2}} = \frac{(X_M^{metal})(X_{FeO}^{silicate})^{n/2}}{(X_{MO_{n/2}}^{silicate})(X_{Fe}^{metal})^{n/2}} \quad (5)$$

in which X is the molar ratio. This method is convenient since the precise definition of oxygen fugacity is not obligatory. On the one hand, the equilibrium constant K_a of the reaction (3) relates to the distribution coefficient K_D:

$$K_a = K_D \times \frac{(\gamma_M^{metal})(\gamma_{FeO}^{silicate})^{n/2}}{(\gamma_{MO_{n/2}}^{silicate})(\gamma_{Fe}^{metal})^{n/2}} \quad (6)$$

where the γ is the activity coefficient of a solute in metal or silicate. The activity coefficient of an element in molten iron can be obtained from the Steelmaking Data Sourcebook (Kagan and Lyubutin 1988), whereas silicate melts lack this data. Generally, the activity coefficient of an element in silicate melts is expressed by a first-order approximation of the melt structure NBO/T (the abbreviation for the molar ratio of non-bridging oxygens to tetrahedrally coordinated cations) (Mysen et al. 1982; Mysen 2003). On the other hand, the equilibrium constant K_a relates to the free energy ΔG° of the reaction (3):

$$\log K_a = -\frac{\Delta G^{\circ}}{RT} = -\frac{\Delta H^{\circ} - T\Delta S^{\circ} + P\Delta V^{\circ}}{RT} \quad (7)$$

where R is the gas constant, P is the pressure, T is the temperature, and ΔH°, ΔS°, and ΔV° are the enthalpy, entropy, and volume change of the reaction, respectively. Finally, the partition coefficient D_M can be expressed as:

$$\log D_M = a + \frac{b}{T} + \frac{c * P}{T} + d * nbo/t - \frac{n * \Delta IW}{2} - \log \frac{(\gamma_M^{metal})}{(\gamma_{Fe}^{metal})^{n/2}} \quad (8)$$

where the regression constants a, b, and c are related to ΔH°, ΔS°, and ΔV°, respectively. In Eq. (8), the partition coefficient of a chemical species is related to the pressure, temperature, oxygen fugacity, and composition of silicate melt and liquid metal. To derive the partitioning behavior of light elements between silicate and metal, the accurate P, T, fO_2, and core composition must be determined first. The following discussion presents a general understanding of the metal-silicate partitioning during Earth's core formation.

Metal-silicate equilibrium under low P–T conditions cannot explain the excess abundance of moderately siderophile elements (MSEs, e.g., Ni, Co, Cu, Mo, and W) in the mantle. In the past few decades, laser-heated diamond anvil cell techniques coupled with micro-zone analysis have significantly boosted high P–T measurements in this research field (Bouhifd and Jephcoat 2011; Siebert et al. 2012, 2013). In these MSEs, Ni and Co have received the most attention due to their poor volatility. However, by extrapolating partition coefficients from low P–T to extremely high P–T conditions, previous studies exhibit large discrepancies for magma ocean depths, ranging from 25 GPa and 2000 K to 60 GPa and 4000 K (Fig. 5) (Righter et al. 1997; Li and Agee 2001; Chabot et al. 2005; Wade and Wood 2005; Siebert et al. 2011). In particular, 45–60 GPa and 3100–3800 K are required to fit the Ni and Co abundance in the mantle, corresponding to a single-stage 1500 km deep magma ocean. In a more realistic model of the continuous core formation (Wade and Wood 2005), the P–T conditions of metal-silicate equilibrium would increase with the increasing magma ocean depth. A depth of silicate-metal equilibrium corresponding to 50–55 GPa is needed to satisfy the Ni and Co abundance in the mantle for the latter model.

Furthermore, the depletion of slightly siderophile elements (SSEs, e.g., V, Cr, Mn, and Nb) in the mantle suggested a much higher equilibrium temperature at present-day oxygen fugacity (Wade and Wood 2005; Corgne et al. 2008, 2009; Siebert et al. 2011). However, such a high temperature would exceed the mantle liquidus and is inconsistent with the scenario that the temperature at the bottom of magma oceans should lay between the liquidus and solidus of silicate mantle. Alternatively, core formation could have occurred under relatively reduced conditions because low fO_2 would enhance the siderophile nature of SSEs. More specifically, the initially accreted materials were reduced with a low fO_2 roughly at IW-4 (< 1 wt% FeO in the silicate mantle). In the history of continuous accretion and core formation, the redox state increased to the present-day ~ IW-2.3 (~ 8 wt% FeO in the silicate mantle). The fO_2 might increase through the following three procedures individually or jointly: (1) accreting materials becoming more oxidized with time (Rubie et al. 2011), (2) oxidization involving replacement reactions of Fe, Si, and O between silicate and metal (Eq. 1) (Wood et al. 2006; Corgne et al. 2008; Javoy et al. 2010), and (3) disproportionation of ferrous iron in perovskite (Frost et al. 2004; Wade and Wood 2005; Trønnes et al. 2019). Contrary to the initially reduced model, Siebert et al. (2013) suggested an initially oxidized model with the fO_2 between IW-1 and IW-2. Besides, it is necessary to note that, as an index of the chemical potential of oxygen, the oxygen fugacity changes with pressure and temperature even if chemical composition does not change (Campbell et al.

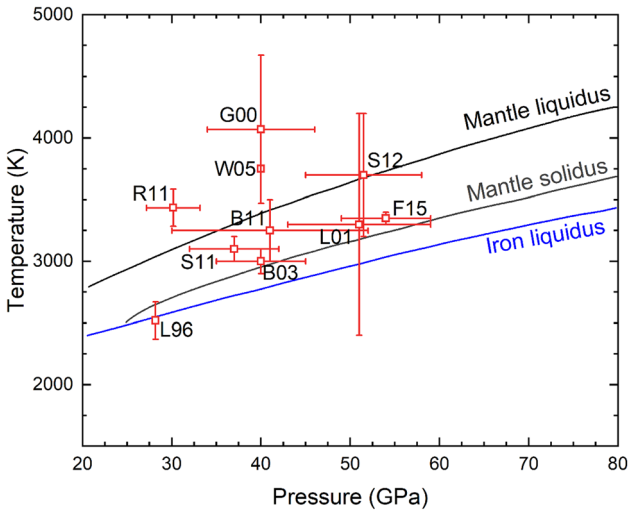

Fig. 5 The core-mantle equilibrium's pressure and temperature conditions to match the present Ni and Co concentrations in the BSE. The single-stage core formation model is adopted with the oxygen fugacity set at around IW-2. The solidus–liquidus temperature of the mantle and the liquidus of iron further constrain the temperature of metal-silicate equilibrium conditions. The silicate mantle's solidus and liquidus curves are from the mean value after Fiquet et al. (2010) and Andrault et al. (2011). The liquidus curve of pure iron is from Anzellini et al. (2013). The square symbols are the P–T solutions suggested from previous works: L96 (Li and Agee 1996), G00 (Gessmann and Rubie 2000), L01 (Li and Agee 2001), B03 (Bouhifd and Jephcoat 2003), W05 (Wade and Wood 2005), B11 (Bouhifd and Jephcoat 2011), R11 (Righter and Chabot 2011), S11 (Siebert et al. 2011), S12 (Siebert et al. 2012), F15 (Fischer et al. 2015)

2009; Righter and Ghiorso 2012; Armstrong et al. 2019; Deng et al. 2020).

Regardless of the fO_2 changing during core formation, Si and O have been proposed as the two predominant light elements in the core (Bouhifd and Jephcoat 2011; Rubie et al. 2011; Siebert et al. 2013; Tsuno et al. 2013). For instance, in the initially reduced model with the fO_2 of IW-3.5, the abundances of Si and O in the core were calculated to be 6.7 and 2.1 wt%, respectively. In the initially oxidized model with the fO_2 of IW-2, Si and O contents in the core were predicted to be 2.2 and 4.5 wt%, respectively. The co-partitioning behavior of Si and O is highly related to *P–T* conditions. At low pressures, the solubilities of Si and O in the metal are very limited and mutually exclusive (Gessmann et al. 2001; Kawazoe and Ohtani 2006). The maximum contents of Si and O in the metal could increase to 11.3 and 8.8 wt% at 100 GPa and 5700 K, respectively (Pigott et al. 2015).

3.2.2 *Chemical partition of light elements H, He, C, N, and S*

How other light elements (e.g., H, He, C, N, and S) were distributed between silicate and metal has been studied using both high *P–T* partitioning experiments and first-principle molecular dynamics (FPMD) simulations. However, high *P–T* experimental data are scarce for now. Sulfur is considered an important light element in the Earth's core (McDonough and Sun 1995; Righter et al. 1997). Thereafter, sulfur partitioning between silicate and metal has been extensively investigated (Li and Agee 2001; Rose-Weston et al. 2009; Boujibar et al. 2014; Suer et al. 2017). Low-pressure experiments (< 25 GPa) showed that sulfur might be more siderophile with increasing pressure and oxygen fugacity, but it could become more lithophile with increasing temperature (Mavrogenes and O'Neill 1999; Rose-Weston et al. 2009; Boujibar et al. 2014). Suer et al. (2017) reported that the partition coefficients of sulfur $D_S^{s/l}$ at high pressures are nearly an order of magnitude less than those results extrapolated from low-pressure experiments (Suer et al. 2017). Consequently, Earth's core likely contains less than 1.2 wt% sulfur based on the current sulfur content in the mantle (maximum 280 ppm) in the homogenous accretion model (Stevenson 1990). On the other hand, 2 wt% sulfur might have partitioned into the core if additional sulfur was added during Earth's final 20% stage of accretion.

FPMD calculations indicate that carbon is moderately siderophile at high *P–T*. The partition coefficient of carbon (D_C) is 9 ± 3 at 40 GPa and 3200 K, resulting in a carbon concentration of 0.15 wt% in the core (Zhang and Yin 2012). A recent partitioning experiment at 37–59 GPa and 4200–5200 K showed consistent D_C values between 1 and 100, corresponding to a maximum of 0.09 ± 0.04 to 0.20 ± 0.10 wt% carbon in the core, respectively (Fischer et al. 2020). On the contrary, the D_C values extrapolated from lower *P–T* experiments are two orders of magnitude more siderophile (Dasgupta et al. 2013; Chi et al. 2014; Armstrong et al. 2015; Li et al. 2016a; Kuwahara et al. 2019; Malavergne et al. 2019). Thus far, the correlation between the D_C values and relevant parameters are controversial. It was reported that the D_C values changed with pressure positively by Dasgupta et al. (2013), negatively by Malavergne et al. (2019), or irrelevantly by Fichtner et al. (2021). High temperature may positively influence the D_C (Li et al. 2015, 2016a), though Fichtner et al. (2021) suggested a negligible temperature dependence. Moreover, the composition and structure of silicate melts may influence the D_C. Fichtner et al. (2021) pointed out the D_C decreased from 640 ± 49 to 14 ± 3 with NBO/T from 1.04 to 3.11, whereas Malavergne et al. (2019) suggested no effect of the NBO/T on the D_C. Interestingly, carbon and hydrogen/silicon appear mutually exclusive in metal liquids, and carbon concentration may decrease with the existence of H in the core (Hirose et al. 2019; Vander Kaaden et al. 2019).

Hydrogen is mainly supposed to be siderophile though debates still exist. Pioneering work on hydrogen partitioning reported the siderophile nature of hydrogen and the positive correlation between *P–T* and partition coefficient D_H (Kuramoto and Matsui 1996). Okuchi (1997) confirmed the siderophile property of hydrogen up to 7 GPa and discovered a stable FeH phase. More recent high *P–T* experiments of hydrogen partitioning between iron and ringwoodite further advocated the siderophile nature of hydrogen (Shibazaki et al. 2009). However, the latest experiments by Clesi et al. (2018) and Malavergne et al. (2019) suggested that hydrogen is lithophile at high pressures to 20 GPa with a low D_H value of ~ 0.2. At the same time, FPMD results indicated the slightly lithophile nature of H with the D_H value of 0.7(1) at 40 GPa and 3200 K (Zhang and Yin 2012). Contrary to the previous simulations, Li et al. (2020) theoretically predicted that hydrogen/water is siderophile under the *P–T* conditions of core formation for both reducing and oxidizing scenarios. It is estimated that $> 75\%$ primitive hydrogen entered the core at 50 GPa and 3500 K. The latest high *P–T* partition experiment also supported the siderophile behavior of hydrogen with the D_H value of greater than 29 at 30–60 GPa and 3100–4600 K (Tagawa et al. 2021). The discrepancy above may be attributed to the instability of the FeH sample at ambient *P–T* conditions and the presence of carbon in metal due to the use of graphite sample capsules in large-volume press experiments. Therefore, hydrogen could escape before the recovered sample is analyzed

(Clesi et al. 2018; Malavergne et al. 2019; Tagawa et al. 2021).

As one of the most abundant elements in the Solar System, nitrogen has also been studied for its partition behavior between metal and silicate. Early studies suggested the moderately siderophile behavior of N at high pressures with D_N values of 1–150 (Kadik et al. 2011; Roskosz et al. 2013; Li et al. 2016b; Yoshioka et al. 2018). FPMD calculations were consistent with the above experimental results with the D_N of 1.8 ± 0.2 at 40 GPa and 3200 K (Zhang and Yin 2012). Furthermore, iron nitrides discovered in superdeep diamond inclusions support siderophile N in the deep Earth (Litasov et al. 2017). However, two recent studies revealed the D_N values heavily depended on oxygen fugacity. Dalou et al. (2017) reported the D_N decreases from 24 ± 3 at IW-0.4 to 0.3 ± 0.1 at IW-3.5, and suggested that nitrogen behaves siderophile at modestly reduced conditions (> IW-2.2) but lithophile at more reduced conditions (< IW-2.2). Additionally, Speelmanns et al. (2019) found that the D_N value decreased to the lithophile side with increasing temperature. It is noted that the above two experiments were performed at relatively low pressures of less than 6 GPa, and those findings need to be evaluated at higher pressures as a function of oxygen fugacity.

The core has been considered a hidden reservoir of noble gases over the past two decades due to high $^3He/^4He$, $^{20}Ne/^{22}Ne$, and $^{36}Ar/^{40}Ar$ in some of the oceanic island basalts (Honda et al. 1991; Graham 2002). Here, we make a brief review focused on He. Pioneer work by Matsuda et al. (1993) concluded that He and other noble gases exhibited a similar partitioning behavior with partition coefficient D values approximately changing from $\sim 4 \times 10^2$ at 0.5 GPa to $\sim 3 \times 10^{-4}$ at 10 GPa. However, recent experiments by Bouhifd et al. (2013) indicated the D_{He} was constant at $\sim 10^{-2}$ up to 40 GPa. The FPMD results by Zhang and Yin (2012) also found that the D_{He} remained nearly constant at $\sim 10^{-2}$ between 20 and 135 GPa at 5000 K, but it was decreased by one order of magnitude to $\sim 10^{-3}$ when decreasing to 3500 K. In short, more work is needed to ascertain the effect of the redox state and silicate/metal composition on the partition behavior of He and other noble gases.

3.2.3 Isotope fractionation during core formation

Isotope fractionation occurs between two phases with different bonding environments, providing constraints on pinning down the species and concentration of light elements in the core (Shahar et al. 2016; Liu et al. 2017). Though the difference between the BSE and chondrites are small, the advances in high-resolution multi-collector inductively-coupled plasma mass spectrometry (MC-ICP-MS) and nuclear resonant inelastic x-ray scattering recently made it possible to detect tiny isotope fractionation of Fe and light elements between silicate and metal (Halliday et al. 2009; Dauphas et al. 2012).

3.2.3.1 Silicon isotopes Georg et al. (2007) argued that the Si isotope difference between the BSE and carbonaceous chondrites is 0.2 ‰, corresponding to 7 wt% Si in the mantle with the metal-silicate equilibrium temperature of 2000 K. Recent studies updated the difference to ∼ 0.1 ‰, provided that the Si isotope composition in chondrites varies from − 0.75 to − 0.36 ‰ (Fitoussi et al. 2009; Ziegler et al. 2010; Armytage et al. 2011). The discrepancy between different research may result from the matrix effects in metal during data collecting in metal and/or the disequilibrium between silicate and metal in experiments (Hin et al. 2014; Bourdon et al. 2018). Therefore, the method still needs to be improved, and more experimental/theoretical work will be undertaken in the future.

3.2.3.2 Carbon isotopes The carbon isotope composition of the BSE is ∼ − 5‰ while those for Mars, Vesta, and chondrites are ∼ − 20 ‰ (Grady et al. 1997; Grady and Wright 2003; Wood et al. 2013). Together with mantle degassing, metal-silicate segregation played a role in carbon isotope fractionation (Satish-Kumar et al. 2011; Horita and Polyakov 2015). However, the carbon isotope fractionation during core formation might be too small (∼ 2.4 ‰) compared with the observed difference between the BSE and the bulk Earth (15 ‰) in a single-stage core formation model. Wood et al. (2013) suggested repeated episodes of equilibrium to solve this problem.

3.2.3.3 Nitrogen isotopes The non-chondritic C/N ratio of the BSE reflects the depletion of nitrogen in the silicate Earth (Marty 2012). Metal-silicate equilibrium during the core formation has been applied to interpret the 'missing nitrogen' mystery, together with high volatilization or the nature of heterogeneously accreted materials. However, there are few studies on nitrogen isotope fractionation during core formation to date (Li et al. 2016b; Dalou et al. 2019). Li et al. (2016b) performed experiments at 1.5–7.0 GPa and 1600–1800 °C, and found the D_N values ranged from 1 to 150 with $\Delta^{15}N^{metal-silicate}$ from − 5.5 to − 1.1‰ (− 3.5 ± 1.7‰, on average). To fit the present-day $\delta^{15}N$ of − 5‰, the metallic core should be substantially deficient in ^{15}N if Earth mainly accreted from enstatite chondrites. Combining the $D_N^{metal-silicate}$, the $\Delta^{15}N^{metal-silicate}$ and the concentration of N of 0.8 ppm in the mantle (Marty 2012), the amount of N in the core is estimated to be 4–16 ppm in the single stage core formation model (Righter

and Chabot 2011), or up to 5000 ppm in the continuous core formation model (Wood et al. 2013). Dalou et al. (2019) performed N partition experiments between Fe–C–N alloy and basaltic melts at 1 GPa and 1400 °C over the oxygen fugacity range of IW-3.1 to IW-0.5. The $\Delta^{15}N^{metal-silicate}$ values were from -257 ± 22 ‰ to -49 ± 1 ‰ over the redox range. The large discrepancy between these two studies may be attributed to the different *P–T* conditions, or perhaps, the disequilibrium in some N isotope fractionation experiments.

3.2.3.4 Sulfur isotopes Sulfur is a siderophile element, and the mass balance rule can constrain its concentration in the core. The mantle contains ~ 200 ppm S based on accessible mantle samples, which only accounts for ~ 3 % of the total S abundance of the solid Earth (Lorand et al. 2013). Thus, there could be ~ 2 wt% S in the core (Dreibus and Palme 1996; McDonough 2014). As for S isotopes, the mantle is depleted in heavy S isotopes. Mantle $^{34}S/^{32}S$ is smaller by 1‰ compared to chondrites, reflecting the effect of core formation on sulfur isotope fractionation (Labidi et al. 2013). The first high *P–T* experiments on sulfur isotope fractionation between metal and silicate were conducted at 1 GPa and 1850 °C, resulting in the $\Delta^{34}S^{metal-silicate}$ of $+2.2 \pm 1.4$ ‰ (Labidi et al. 2016). This pioneering work suggested that the S isotope fractionation factor is highly dependent on the structure of silicate melts, especially the strength of sulfur bonding. The $\Delta^{34}S^{metal-silicate}$ values change from $+0.2 \pm 0.1$ ‰ to $+1.4 \pm 0.2$ ‰ with increasing boron and aluminum concentration in silicate melts at 1–1.5 GPa and 1650 °C. Based on the above-mentioned isotopic estimates, 85% to 97% of the bulk S should be contained in Earth's core, which agrees well with the cosmochemical estimates. Nevertheless, further studies are needed to better understand the contributions of late veneer accretion, degassing, and silicate crystallization on the concentration of S isotopes in the mantle.

3.2.3.5 Hydrogen isotopes The δD of the BSE and carbonaceous chondrites are close to each other (-37 ‰ and -101 ± 60 ‰, respectively) (Hallis 2017). Therefore, the source of most hydrogen or water on Earth is believed to be CI carbonaceous chondrite-like materials. Other sources including cometary water or solar nebula gas show much different H isotope compositions, $+926$ ‰ and -865 ‰, respectively (Geiss and Gloeckler 1998; Altwegg et al. 2015). The difference of H isotope compositions between the BSE and CI chondrites indicates that some H partitioned into the core (Andreev and Magomedbekov 2001). The hydrogen concentration in the core has been probed through geochemical and cosmochemical aspects, but those results conflict with each other (Wood et al. 2006; Zhang and Yin 2012; McDonough 2014; Clesi et al. 2018). Wu et al. (2018) proposed a model of hydrogen storage and isotope fractionation between the mantle and core by parameterizing the isotopic fractionation factor and initial bulk δD value of chondrites. In this model, the best fit revealed that ~ 7–8 oceans H could have been accreted from chondrites, in which 5 oceans H are in the core with the δD of -230‰ (D/H of 120×10^{-6}) and 3 oceans H are in the BSE with the δD of -37 ‰ (D/H of 150×10^{-6}).

3.2.3.6 Iron isotopes Fe isotope concentration was first detected for chondrites and silicate samples (basalts and peridotites), but no significant difference was present (Poitrasson et al. 2004; Weyer et al. 2005; Williams et al. 2006; Craddock et al. 2013; Teng et al. 2013; Sossi et al. 2016). Similarly, experiments and calculations were also performed to figure out the Fe isotope fractionation between silicate and metal (Polyakov 2009; Hin et al. 2012; Shahar et al. 2016; Elardo and Shahar 2017; Liu et al. 2017). In general, earlier studies found no obvious Fe isotope fractionations between silicate and metal alloys. Liu et al. (2017) found no significant Fe isotope fractionation between silicates and iron-rich alloys (H, C, O, Si, Ni, and S). Nuclear resonant inelastic x-ray scattering measures on iron and iron-rich alloys were consistent between Shahar et al. (2016) and Liu et al. (2017), except for the difference in mantle bridgmanite and melt. In addition, Ni may play an important role in the Fe isotope fractionation between iron alloys and silicate melts (Elardo and Shahar 2017).

3.3 Geophysical constraints

Apart from geochemical and cosmochemical signatures (e.g., elemental partitioning and isotopic fractionation of light elements), the physical properties of iron-rich alloys provide powerful constraints on the species and abundance of light elements in the Earth's core.

3.3.1 Density and velocity of Fe-light element alloys

It serves as an important constraint on the Earth's core composition that the compressibility and density-velocity profiles of iron-rich alloys under high *P–T* conditions are compared with observed seismic models, such as the preliminary reference Earth model (PREM) and AK135 model (Dziewonski and Anderson 1981; Kennett et al. 1995). The density-pressure profiles of liquid iron alloyed with S, Si, C, O, and H have been measured by using a battery of probes, including the sink/float method (Nishida et al. 2008; Tateyama et al. 2011), x-ray absorption method

(Sanloup et al. 2011; Chen et al. 2014b; Zhu et al. 2021), x-ray diffuse scattering analysis (Morard et al. 2013), shock-wave experiments (Zhang et al. 2014; Huang et al. 2019), and ab initio calculations (Ichikawa and Tsuchiya 2020). Sata et al. (2010) found that the incorporation of light elements (Si, O, S, and C) reduces the density and enhances the compressibility of pure Fe (Fig. 6). However, Si only shows a small effect on the density/compressibility on pure Fe compared with other light elements. It is likely due to the difference in atomic site occupation. Si substitutes for Fe while S, H, and C occupy interstitial sites (Waseda et al. 1980; Ikuta et al. 2019).

The velocity–pressure (density) profiles of iron and iron-rich alloys have been extensively investigated at high pressure using shock wave techniques, inelastic x-ray scattering, picosecond acoustics, and ab initio calculations (Lin et al. 2005; Kantor et al. 2007; Vočadlo et al. 2009; Mao et al. 2012; Chen et al. 2014a, 2018; Decremps et al. 2014; Zhang et al. 2014; Antonangeli and Ohtani 2015; Ohtani et al. 2015; Prescher et al. 2015; Liu et al. 2016a; Lai et al. 2020) (Fig. 6). For now, the measurements of velocity under simultaneously high *P*–*T* conditions are still challenging. Instead, most of the velocity–pressure (density) data were reported at room temperature and extrapolated to the core conditions using Birch's law (Birch 1964). The incorporation of light elements shifts the velocity-density profile of pure iron under the core conditions. However, the reliability of Birch's law under high temperature is of debate (Lin et al. 2005; Gao et al. 2008). Recently, Mao et al. (2012) and Liu et al. (2014) suggested that the empirical power-law function better fits the velocity-density data. To date, many potential assemblies of light elements have been suggested to exist in the core, including Fe–9.5S–0.5O (Huang et al. 2011), Fe–5Ni–6S–2Si (Morard et al. 2013), Fe–9Ni–10Si (Zhang et al. 2014), and Fe–3.7O–1.9Si (Badro et al. 2014) (all the values are in wt%). In short, S, Si, and O tend to be the most important light elements in the core. However, the conclusion is not unique, and multiple interdisciplinary constraints need to be further evaluated.

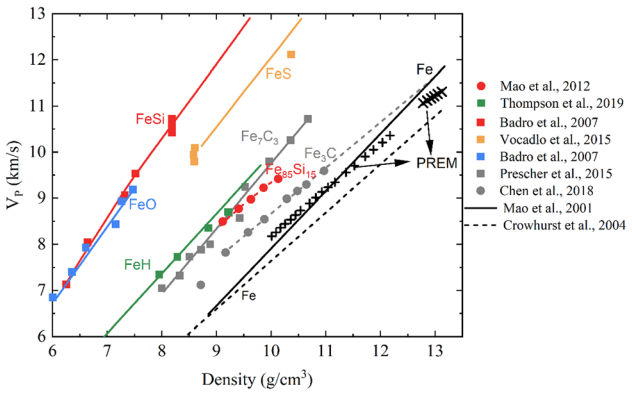

Fig. 6 The density and V_P for Fe-rich alloys. The colored squares and circles are measured data for Fe-rich alloys, while the colored curves fit the Birch's law. The solid and dashed curves in black represent pure iron. The crosses are the outer core and inner core. The datasets are from Mao et al. (2012), Litasov and Shatskiy (2016), Chen et al. (2018), Thompson et al. (2018), and references therein

3.3.2 Melting reduction of light elements

In addition to the density and velocity, light elements also affect the melting temperature of Fe. The melting temperature of liquid outer core materials provides a lower bound of the core-mantle boundary (CMB) temperature. The solidus temperature of mantle peridotite was used to set the upper boundary of the temperature at the CMB (Garnero et al. 2016; Morard et al. 2017). A reasonable estimate of the CMB temperature boundary is 3750–4200 K (Fiquet et al. 2010; Andrault et al. 2014; Pradhan et al. 2015; Morard et al. 2017). Therefore, the reduction of melting temperature due to the presence of light elements could constrain the outer core composition.

The solidus temperature of the iron-rich Fe-light element (Fe–X) binary system could be estimated by linearly linking the melting point of pure iron and the eutectic melting point of the Fe–X system (Morard et al. 2017). At the CMB depth (136 GPa), the melting temperature of pure iron could be as high as 4200 K (Anzellini et al. 2013). Additionally, the eutectic melting temperatures of Fe–Si, Fe–O, Fe–C, Fe-S at 136 GPa are 4300 K with 18 at% Si, 2870 K with 15 at% S, 2990 K with 11 at% C, 3200 K with 30 at% O (Morard et al. 2011, 2017; Fei and Brosh 2014; Lord et al. 2014) (Fig. 7). Notably, the geotherm of the outer core should be higher than the melting curve. Otherwise the outer core would be solid now. A temperature jump between the geotherm and the melting curve of outer-core liquid is estimated to be 400–900 K at the CMB (Anzellini et al. 2013; Komabayashi 2014).

The accretion and metal/silicate partitioning studies suggested that Si or O was the major light element in the core (Siebert et al. 2013; Fischer et al. 2015). However, the melting temperature of the binary Fe–Si system is too high to keep the bottom mantle in a solid state. Considerable amounts of C or S or a large amount of O (at least 2 wt% C/S or 5 wt% O) are needed to reduce the melting temperature of outer core materials, which is supposed to be lower than the mantle solidus at the CMB (Morard et al. 2017). Kim et al. (2020) reported the lowest solidus temperature of anhydrous pyrolytic material as low as 3430 K at 136 GPa, about 700 K lower than the previous estimates. The lower solidus temperature of mantle materials implies more light elements in the outer core (more than 4 wt% C/S or 10 wt% O for a binary Fe–X system). The present-day outer core probably contains more than one kind of

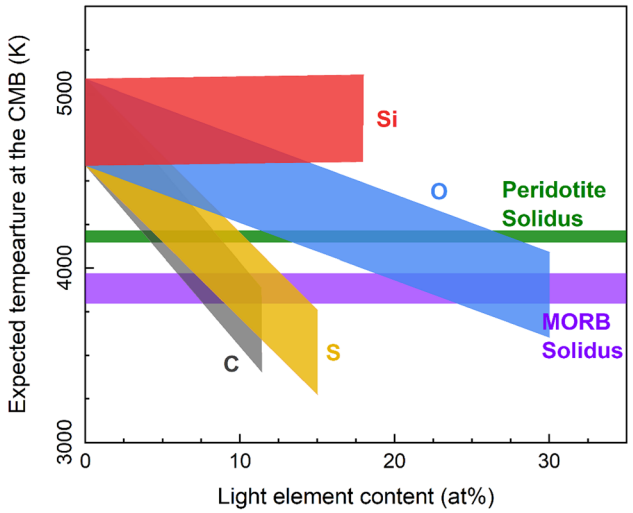

Fig. 7 Melting temperature reduction of light elements at the CMB. The liquidus temperature of pure Fe is from Anzellini et al. (2013). The eutectic melting points and eutectic compositions for C, S, O, and Si are from Morard et al. (2017). The expected temperature of Fe–X binary systems for the outer core is shifted up by ΔT = 400–900 K to account for the temperature difference between the adiabat and melting curve of the outer core. The temperature of the outer core at the CMB can be restricted by the solidus of peridotite and mid-ocean ridge basalt (MORB) (Fiquet et al. 2010; Andrault et al. 2014; Pradhan et al. 2015)

light element. The nonlinear interactions of multiple light elements in the core may further decrease the melting temperature of Fe alloys.

3.3.3 Liquidus phase relations of iron-rich alloys

The chemical composition of the inner core is vital to constrain the outer core since the former is growing out of the latter. Chen et al. (2014a) and Prescher et al. (2015) suggested Fe_7C_3 to be the main component of the inner core, but the latest study implied that Fe_7C_3 is too light for the inner core (Li et al. 2016c). More importantly, the density jump across the inner core boundary (ICB) indicates that the solid inner core is relatively depleted in light elements compared to the liquid outer core (Masters and Gubbins 2003; Ichikawa et al. 2014). As for the Fe–X binary systems, more constraints can be provided according to their liquidus phase relations. The liquidus field of iron decreases in the Fe–C (Lord et al. 2009; Liu et al. 2016b; Mashino et al. 2019), Fe-S (Kamada et al. 2012; Mori et al. 2017), and Fe–Si (Ozawa et al. 2016) binary liquids with increasing pressure, but expands in the Fe–O system (Oka et al. 2019). None of Si, C, or S could be the dominant light element in the inner core because the content of these elements is not enough to support the density jump across the ICB in a binary Fe–X system (Oka et al. 2019). Additionally, O cannot be the solo light element in the inner core due to the limited solubility of O in solid Fe up to 0.1 wt% at 330 GPa (Ozawa et al. 2010). Nevertheless, a certain amount of O should exist in the core according to the accretion and core formation models (Siebert et al. 2013; Fischer et al. 2015) and FPMD calculations (Badro et al. 2014; Li et al. 2018).

A recent review summarized the standard Fe–X binary systems and found that none of the binary systems can account for all the properties of Earth's core (Komabayashi 2021). The ternary Fe–X–Y alloy systems have been suggested as the component of the core in recent years, including Fe–Si–O, Fe–S–O, Fe–C–H, and Fe–Si–C (Antonangeli et al. 2010; Hirose et al. 2017; Tateno et al. 2018; Mashino et al. 2019; Yokoo et al. 2019; Miozzi et al. 2020; Hasegawa et al. 2021). Strong interactions between light elements occur in these alloy systems, altering the solubility of light elements and even resulting in liquid–liquid immiscibility (Hasegawa et al. 2021). For instance, SiO_2 forms in the Fe–Si–O ternary alloy liquid as it cools because of the wide liquidus field of silica in the system (Hirose et al. 2017). If Si is an essential component in the outer core, some C or S should also be included to fit the density and velocity of the seismic model (Li et al. 2018). On the other hand, O is a plausible light component in the outer core because its low solubility in the solid Fe could explain the density jump across the ICB. In this scheme, a S-poor (0–3 wt%) and O-rich (4–5.5 wt%) outer core, or a C-bearing, S-poor, and O-rich ($Fe_{84}S_{3.4}O_{8.4}C_{4.2}$, $Fe_{83.2}S_{1.1}O_{8.2}C_{7.5}$) outer core could satisfy the criteria of density and velocity simultaneously (Badro et al. 2014; Li et al. 2018).

4 Other terrestrial planets and small planetary bodies

4.1 Mercury

Mercury is the densest and smallest terrestrial planet in the Solar System (Anderson et al. 1987). The MESSENGER (2008–2015) mission provided detailed structure information about Mercury: a crust of ~ 50 km, a mantle of ~ 260 km, and a core of ~ 2030 km (Margot et al. 2012; Smith et al. 2012; Zuber et al. 2012). The high S (3.5 wt%) (Namur et al. 2016) and low FeO (1.5 wt%) (Nittler et al. 2011) contents of the surface are attributed to the highly reduced accretion and differentiation history of Mercury (Nittler et al. 2011; McCubbin et al. 2012). Mercury's redox condition (IW-7.3 to IW-4.5) is so reduced that a large portion of Si would partition into the core since Si becomes siderophile under reduced conditions (Malavergne et al. 2010; Zolotov et al. 2013). A S-rich layer should be extracted from the core since Fe–Si-S displays

liquid immiscibility at the silicate-metal equilibrium pressures (4–7 GPa) and temperatures above the liquidus temperature (Morard and Katsura 2010; Hauck et al. 2013). The Si content in the core is estimated to be 15 wt% based on geophysical models (Margot et al. 2018) or 20 wt% based on the partition coefficient of Si (Cartier and Wood 2019). The S content in the core is estimated to be below 1.5 wt% assuming the bulk S content for Mercury is ~ 4 wt% (Nittler et al. 2011; Namur et al. 2016) (Table 2). Meanwhile, some amount of carbon has been suggested in the core, possibly at the wt% level, to satisfy the density and bulk composition of Mercury; however, the abundance of carbon is highly anticorrelated with silicon in iron-dominated core (Cartier and Wood 2019; Vander Kaaden et al. 2019; Knibbe et al. 2021).

4.2 Venus

Venus is often thought to be Earth's sister planet because of its similar mass, density, and orbit radii (Taylor et al. 2018). The main difference is a late (~ 95 ± 32 Ma) giant impact on Earth that did not exist for Venus (Jacobson et al. 2014). The core composition is also affected by the impact mixing efficiency (Zube et al. 2019). Thus far, there are few constraints on the core composition of Venus. Trønnes et al. (2019) estimated the light elements in Venus's core to be 6.2 wt% Si and 2.5 wt% O based on the extrapolation from the composition of Mercury and Earth.

4.3 Mars

Mars is identified as the source of many meteorites, including the Shergotty-Nakhla-Chassiny (SNC) group. Radioisotope data of Martian meteorites show that the accretion and differentiation of Mars took place rapidly (Dauphas and Pourmand 2011; Bouvier et al. 2018). The composition of meteorites also provides a cosmochemical constraint on the composition of Mars. The Wänke and Dreibus model family is the mostly accepted compositional model of Mars (Morgan and Anders 1979; Dreibus and Wänke 1987; Wänke and Dreibus 1988; Halliday et al. 2001; Taylor 2013). Later studies provided compositional models from an isotopic approach by matching the O isotope composition of SNC's to mixtures of chondrites (Lodders and Fegley 1997; Sanloup et al. 1999). A third way is a geophysical approach to construct the mineralogy of the interior of Mars, though the geophysical data of Mars is still lacking (Khan and Connolly 2008; Khan et al. 2018; Giardini et al. 2020; Stähler et al. 2021). Sulfur is suggested to be the dominant light element in the core because of its siderophile property at the P–T-fO_2 conditions relevant to Martian core formation (Lodders and Fegley 1997; Taylor 2013; Steenstra and van Westrenen 2018; Brennan et al. 2020). For example, Brennan et al. (2020) suggested 18–19 wt% S in the Martian core based on a multi-stage model of Martian core formation. Si partitions in the Martian core at a trace lever due to the slightly siderophile property at the Martian core's low P–T and high fO_2 conditions (Fischer et al. 2015; Brennan et al. 2020). C and H contents in the core are rarely constrained, but their solubilities are reduced in a S-rich alloy system. There would be less than 0.5 wt% C and 60 ppm H in the core if 16 wt% S is present (Clesi et al. 2018; Tsuno et al. 2018). As for the O, most studies suggested the maximum content of ~ 1 wt% due to the modest P–T conditions of metal-silicate equilibrium (Ricolleau et al. 2011; Fischer et al. 2015; Brennan et al. 2020). However, other studies preferred an O content of a few percent high, assuming a high

Table 2 Core formation conditions and potential light elements in terrestrial planets

	Core fraction (wt%)	CMB pressure (GPa)	Bulk fO_2 (ΔIW)	Core composition (wt%)			
				Si	O	S	
Mercury	67	5.7	− 4.56	15–20		1.5	Margot et al. (2018) and Cartier and Wood (2019)
Venus	29	114	− 2.41	6.2	2.5		Aitta (2012) and Trønnes et al. (2019)
				1.0	3.9		
Earth[a]	33	136	− 2.21	5.1	2.6	1.9	McDonough (2014), Badro et al. (2015) and Fischer et al. (2015)
Moon	2	4.8	− 1.87			6	Weber et al. (2011)
Mars	21	20	− 1.36		1	18	Brennan et al. (2020)
					5	10–15	Stähler et al. (2021)
Vesta	18	0.1	− 1.10			12.8–16	Toplis et al. (2013)

Core fraction, CMB pressure, and oxygen fugacity data follow those from Trønnes et al. (2019) and references therein

[a]The composition is inferred from the multiple constraints of cosmochemistry, metal-silicate partitioning, and geophysics

P–T condition for the equilibrium of metal and silicate (Tsuno et al. 2011; Yoshizaki and McDonough 2020). Recently, it was estimated the radius of the liquid Martian core is as large as 1830 ± 40 km and the mean density is 5.7 to 6.3 g/cm^3 based on the Interior Exploration using Seismic Investigations, Geodesy, and Heat Transport (InSight) mission (Cottaar and Koelemeijer 2021; Stähler et al. 2021). Abundant S is required to reduce the density to the observed value for a Fe-S Martian core model. The amount of S needed based on Martian seismic observations exceeds that constrained by geochemical and cosmochemical models (< 19 wt%) and the S content of the most S-abundant EH chondrites (Steenstra and van Westrenen 2018; Brennan et al. 2020). Therefore, other light elements including O, C, and/or H may be added to satisfy the low density of Martian core. A combination of 10–15 wt% S, 5 wt% O, 1 wt% C, and 1 wt% H has been suggested as the upper limits to jointly satisfy constraints from geophysical, geochemical, and cosmochemical aspects (Stähler et al. 2021).

4.4 Moon

As the only satellite of Earth, the Moon formed from the giant impact event. Seismic observation reveals that a solid inner core and a liquid outer core exist in the Moon, overlain by a partially molten boundary layer (Weber et al. 2011). Light elements are required in the liquid core for the density deficiency, but the species and content of light elements are still debated (Weber et al. 2011; Righter et al. 2017; Garcia et al. 2019). C and S are the most likely candidates because of the observation of S and C from lunar samples and the partitioning properties of C and S between silicate and metal (Chi et al. 2014; Righter et al. 2017; Steenstra and van Westrenen 2017). Si and O are unlikely to be the dominant light elements due to their low partition coefficients during the lunar core formation (Ricolleau et al. 2011). C is weak in reducing the density of Fe alloys compared to S (Zhu et al. 2021). If C is the only light element in the lunar core, the Fe–C density cannot be reduced to the seismically observed value even at the eutectic point (Fei and Brosh 2014). If S is the only light element, 10–27 wt% S is needed to meet the observed density while no more than 6 wt% S is needed to meet the liquidus temperature of the lunar core (Morard et al. 2008; Garcia et al. 2019). However, some new works using geochemical constraints suggest a low S and C lunar core (Righter et al. 2017; Steenstra et al. 2018).

4.5 Vesta

The asteroid 4-Vesta is the parent body of HED (howardite, eucrite, diogenite) meteorites (McCord et al. 1970; Scott et al. 2009). Radiogenic isotope research on the HED meteorites indicated that the core-mantle differentiation in Vesta takes place within the first 2.5 ± 1.2 Ma after forming CAIs (Touboul et al. 2015; Hublet et al. 2017). The depleted siderophile elements in HED and the gravitational moment J_2 of 0.03178 also prove the existence of a metallic core (Palme and Rammensee 1981; Holzheid and Palme 2007; Russell et al. 2012). The *P–T-*fO_2-composition conditions during the core formation have been studied based on the siderophile element depletion, isotopic composition, and thermo-chemical modeling (Holzheid and Palme 2007; Pringle et al. 2013; Neumann et al. 2014; Steenstra et al. 2016; Kiefer and Mittlefehldt 2017). The equilibrium condition has atmospheric pressure, 1725–1850 K, and IW-2.30 ± 0.15. The main light element in the core is sulfur, up to 12.8 wt% or 16 wt% corresponding to the bulk composition of H chondrite or 3/4 H + 1/4 CM chondrites, respectively (Toplis et al. 2013; Steenstra et al. 2016, 2019).

5 The way forward

We have reviewed the various scenarios of terrestrial planet formation and differentiation, and the current understandings of light elements in the iron-rich core. In the past few decades, many remarkable achievements have significantly promoted the knowledge frontiers of the deep interiors and evolution of Earth and other terrestrial planets. However, many mysteries and contradictions remain in the existing literature. Further exploration and novel methods are required to overcome the obstacles ahead, including.

(1) Reliable experimental conditions. For instance, stable and homogenous *P–T* conditions are essential for the chemical equilibrium between metal and silicate. Moreover, the latter is necessary to obtain precise partitioning coefficients for light elements.
(2) The Fe–X–Y ternary system or multiple systems. More than one kind of light element likely exists present in iron-rich cores. Thus, traditional studies on the Fe–X binary systems are outdated to some extent.
(3) Coupling of chemical and physical constraints. Fe-rich compounds constrained by high-pressure mineral physics may not be realistic from cosmochemical and geochemical aspects. However, the combination of chemical and physical constraints can provide more reasonable estimates for the light matter in the core.
(4) Exploration of other terrestrial planets and asteroids. The ongoing exploration of the Moon and Mars will

update our understanding of the general rules of planet formation and differentiation. In addition, new knowledge can be obtained by comparing the similarities and differences between terrestrial planets and other interstellar objects.

(5) Novel computing technologies. With the development of computation, many advances have been made in these research fields. For example, the emerging research model overlaps of machine learning with numerical modeling, seismicity, crystal structure prediction algorithms, and many others. Thus, using new computational techniques can help gain a better understanding of the evolution of terrestrial planets.

Acknowledgements We thank Yuan Li and the other anonymous reviewer(s) for their constructive comments and suggestions. This work is supported by the National Natural Science Foundation of China (NSFC grant No. 42072052).

Declarations

Conflict of interest The authors declare that they have no competing interests.

References

Aitta A (2012) Venus' internal structure, temperature and core composition. Icarus 218:967–974

Allègre CJ, Poirier J-P, Humler E, Hofmann AW (1995) The chemical composition of the Earth. Earth Planet Sci Lett 134:515–526

Altwegg K, Balsiger H, Bar-Nun A, Berthelier JJ, Bieler A, Bochsler P et al (2015) 67P/Churyumov-Gerasimenko, a Jupiter family comet with a high D/H ratio. Science 347:1261952

Andrault D, Bolfan-Casanova N, Nigro GL, Bouhifd MA, Garbarino G, Mezouar M (2011) Solidus and liquidus profiles of chondritic mantle: implication for melting of the Earth across its history. Earth Planet Sci Lett 304:251–259

Andrault D, Pesce G, Bouhifd MA, Bolfan-Casanova N, Henot JM, Mezouar M (2014) Melting of subducted basalt at the core-mantle boundary. Science 344:892–895

Andreev BM, Magomedbekov EP (2001) Separation of hydrogen isotopes by chemical isotope exchange in systems involving metal and intermetallic compound hydrides. Sep Sci Technol 36:2027–2086

Antonangeli D, Ohtani E (2015) Sound velocity of hcp-Fe at high pressure: experimental constraints, extrapolations and comparison with seismic models. Prog Earth Planet Sci 2:1–11

Antonangeli D, Siebert J, Badro J, Farber DL, Fiquet G, Morard G, Ryerson FJ (2010) Composition of the Earth's inner core from high-pressure sound velocity measurements in Fe–Ni–Si alloys. Earth Planet Sci Lett 295:292–296

Anzellini S, Dewaele A, Mezouar M, Loubeyre P, Morard G (2013) Melting of iron at Earth's inner core boundary based on fast X-ray diffraction. Science 340:464–466

Armstrong LS, Hirschmann MM, Stanley BD, Falksen EG, Jacobsen SD (2015) Speciation and solubility of reduced C–O–H–N volatiles in mafic melt: implications for volcanism, atmospheric evolution, and deep volatile cycles in the terrestrial planets. Geochim Cosmochim Acta 171:283–302

Armstrong K, Frost DJ, McCammon CA, Rubie DC, Boffa Ballaran T (2019) Deep magma ocean formation set the oxidation state of Earth's mantle. Science 365:903–906

Armytage R, Georg R, Savage P, Williams H, Halliday A (2011) Silicon isotopes in meteorites and planetary core formation. Geochim Cosmochim Acta 75:3662–3676

Badro J, Cote AS, Brodholt JP (2014) A seismologically consistent compositional model of Earth's core. Proc Natl Acad Sci 111:7542–7545

Badro J, Brodholt JP, Piet H, Siebert J, Ryerson FJ (2015) Core formation and core composition from coupled geochemical and geophysical constraints. Proc Natl Acad Sci 112:12310–12314

Barboni M, Boehnke P, Keller B, Kohl IE, Schoene B, Young ED, McKeegan KD (2017) Early formation of the Moon 4.51 billion years ago. Sci Adv 3:e1602365

Birch F (1964) Density and composition of mantle and core. J Geophys Res 69:4377–4388

Blum J, Wurm G (2008) The growth mechanisms of macroscopic bodies in protoplanetary disks. Ann Rev Astron Astrophys 46:21–56

Bollard J, Connelly JN, Whitehouse MJ, Pringle EA, Bonal L, Jørgensen JK et al (2017) Early formation of planetary building blocks inferred from Pb isotopic ages of chondrules. Sci Adv 3:e1700407

Bouhifd MA, Jephcoat AP (2003) The effect of pressure on partitioning of Ni and Co between silicate and iron-rich metal liquids: a diamond-anvil cell study. Earth Planet Sci Lett 209:245–255

Bouhifd MA, Jephcoat AP (2011) Convergence of Ni and Co metal–silicate partition coefficients in the deep magma-ocean and coupled silicon–oxygen solubility in iron melts at high pressures. Earth Planet Sci Lett 307:341–348

Bouhifd MA, Jephcoat AP, Heber VS, Kelley SP (2013) Helium in Earth's early core. Nat Geosci 6:982–986

Boujibar A, Andrault D, Bouhifd MA, Bolfan-Casanova N, Devidal J-L, Trcera N (2014) Metal–silicate partitioning of sulphur, new experimental and thermodynamic constraints on planetary accretion. Earth Planet Sci Lett 391:42–54

Bourdon B, Roskosz M, Hin RC (2018) Isotope tracers of core formation. Earth Sci Rev 181:61–81

Bouvier LC, Costa MM, Connelly JN, Jensen NK, Wielandt D, Storey M et al (2018) Evidence for extremely rapid magma ocean crystallization and crust formation on Mars. Nature 558:586–589

Brasser R, Dauphas N, Mojzsis SJ (2018) Jupiter's influence on the building blocks of Mars and Earth. Geophys Res Lett 45:5908–5917

Brennan MC, Fischer RA, Irving JCE (2020) Core formation and geophysical properties of Mars. Earth Planet Sci Lett 530:115923

Campbell AJ, Danielson L, Righter K, Seagle CT, Wang Y, Prakapenka VB (2009) High pressure effects on the iron–iron oxide and nickel–nickel oxide oxygen fugacity buffers. Earth Planet Sci Lett 286:556–564

Canup RM (2008) Lunar-forming collisions with pre-impact rotation. Icarus 196:518–538

Carlson RW, Garnero E, Harrison TM, Li J, Manga M, McDonough WF et al (2014) How did early Earth become our modern world? Annu Rev Earth Planet Sci 42:151–178

Carlson RW, Brasser R, Yin Q-Z, Fischer-Gödde M, Qin L (2018) Feedstocks of the terrestrial planets. Space Sci Rev 214:121–153

Cartier C, Wood BJ (2019) The role of reducing conditions in building Mercury. Elements 15:39–45

Chabot NL, Draper DS, Agee CB (2005) Conditions of core formation in the earth: constraints from nickel and cobalt partitioning. Geochim Cosmochim Acta 69:2141–2151

Chen B, Li Z, Zhang D, Liu J, Hu YM, Zhao J et al (2014a) Hidden carbon in Earth's inner core revealed by shear softening in dense Fe_7C_3. Proc Natl Acad Sci 111:17755–17758

Chen J, Yu T, Huang S, Girard J, Liu X (2014b) Compressibility of liquid FeS measured using X-ray radiograph imaging. Phys Earth Planet Inter 228:294–299

Chen B, Lai X, Li J, Liu J, Zhao J, Bi W et al (2018) Experimental constraints on the sound velocities of cementite Fe_3C to core pressures. Earth Planet Sci Lett 494:164–171

Chi H, Dasgupta R, Duncan MS, Shimizu N (2014) Partitioning of carbon between Fe-rich alloy melt and silicate melt in a magma ocean— implications for the abundance and origin of volatiles in Earth, Mars, and the Moon. Geochim Cosmochim Acta 139:447–471

Clesi V, Bouhifd MA, Bolfan-Casanova N, Manthilake G, Schiavi F, Raepsaet C et al (2018) Low hydrogen contents in the cores of terrestrial planets. Sci Ances 4:e1701876

Connelly JN, Bizzarro M, Krot AN, Nordlund Å, Wielandt D, Ivanova MA (2012) The absolute chronology and thermal processing of solids in the solar protoplanetary disk. Science 338:651–655

Connelly JN, Schiller M, Bizzarro M (2019) Pb isotope evidence for rapid accretion and differentiation of planetary embryos. Earth Planet Sci Lett 525:115722

Corgne A, Keshav S, Wood BJ, McDonough WF, Fei Y (2008) Metal–silicate partitioning and constraints on core composition and oxygen fugacity during Earth accretion. Geochim Cosmochim Acta 72:574–589

Corgne A, Siebert J, Badro J (2009) Oxygen as a light element: a solution to single-stage core formation. Earth Planet Sci Lett 288:108–114

Cottaar S, Koelemeijer P (2021) The interior of Mars revealed. Science 373:388–389

Craddock PR, Warren JM, Dauphas N (2013) Abyssal peridotites reveal the near-chondritic Fe isotopic composition of the Earth. Earth Planet Sci Lett 365:63–76

Cuzzi JN, Dobrovolskis AR, Champney JM (1993) Particle-gas dynamics in the midplane of a protoplanetary nebula. Icarus 106:102–134

Cuzzi JN, Hogan RC, Shariff K (2008) Toward planetesimals: dense chondrule clumps in the protoplanetary nebula. Astrophys J 687:1432

Dalou C, Hirschmann MM, von der Handt A, Mosenfelder J, Armstrong LS (2017) Nitrogen and carbon fractionation during core-mantle differentiation at shallow depth. Earth Planet Sci Lett 458:141–151

Dalou C, Furi E, Deligny C, Piani L, Caumon M-C, Laumonier M et al (2019) Redox control on nitrogen isotope fractionation during planetary core formation. Proc Natl Acad Sci 116:14485–14494

Dasgupta R, Chi H, Shimizu N, Buono AS, Walker D (2013) Carbon solution and partitioning between metallic and silicate melts in a shallow magma ocean: implications for the origin and distribution of terrestrial carbon. Geochim Cosmochim Acta 102:191–212

Dauphas N (2017) The isotopic nature of the Earth's accreting material through time. Nature 541:521–524

Dauphas N, Pourmand A (2011) Hf–W–Th evidence for rapid growth of Mars and its status as a planetary embryo. Nature 473:489–492

Dauphas N, Roskosz M, Alp EE, Golden DC, Sio CK, Tissot FLH et al (2012) A general moment NRIXS approach to the determination of equilibrium Fe isotopic fractionation factors: application to goethite and jarosite. Geochim Cosmochim Acta 94:254–275

Decremps F, Antonangeli D, Gauthier M, Ayrinhac S, Morand M, Marchand GL et al (2014) Sound velocity of iron up to 152 GPa by picosecond acoustics in diamond anvil cell. Geophys Res Lett 41:1459–1464

DeMeo FE, Carry B (2014) Solar System evolution from compositional mapping of the asteroid belt. Nature 505:629–634

Deng J, Du Z, Karki BB, Ghosh DB, Lee KKM (2020) A magma ocean origin to divergent redox evolutions of rocky planetary bodies and early atmospheres. Nat Commun 11:2007

Dominik C, Blum J, Cuzzi JN, Wurm G (2007) Growth of dust as the initial step toward Planet Formation. University of Arizona Press

Dreibus G, Palme H (1996) Cosmochemical constraints on the sulfur content in the Earth's core. Geochim Cosmochim Acta 60:1125–1130

Dreibus G, Wänke H (1987) Volatiles on Earth and Mars: a comparison. Icarus 71:225–240

Dubrulle B, Morfill G, Sterzik M (1995) The dust subdisk in the protoplanetary nebula. Icarus 114:237–246

Dziewonski AM, Anderson DL (1981) Preliminary reference Earth model. Phys Earth Planet Inter 25:297–356

Elardo SM, Shahar A (2017) Non-chondritic iron isotope ratios in planetary mantles as a result of core formation. Nat Geosci 10:317–321

Elkins-Tanton LT (2012) Magma oceans in the inner Solar System. Annu Rev Earth Planet Sci 40:113–139

Fei Y, Brosh E (2014) Experimental study and thermodynamic calculations of phase relations in the Fe–C system at high pressure. Earth Planet Sci Lett 408:155–162

Fichtner CE, Schmidt MW, Liebske C, Bouvier A-S, Baumgartner LP (2021) Carbon partitioning between metal and silicate melts during Earth accretion. Earth Planet Sci Lett 554:116659

Fiquet G, Auzende A, Siebert J, Corgne A, Bureau H, Ozawa H, Garbarino G (2010) Melting of peridotite to 140 gigapascals. Science 329:1516–1518

Fischer RA, Nakajima Y, Campbell AJ, Frost DJ, Harries D, Langenhorst F et al (2015) High pressure metal–silicate partitioning of Ni Co, V, Cr, Si, and O. Geochim Cosmochim Acta 167:177–194

Fischer RA, Cottrell E, Hauri E, Lee KKM, Le Voyer M (2020) The carbon content of Earth and its core. Proc Natl Acad Sci 117:8743–8749

Fitoussi C, Bourdon B, Kleine T, Oberli F, Reynolds BC (2009) Si isotope systematics of meteorites and terrestrial peridotites: implications for Mg/Si fractionation in the solar nebula and for Si in the Earth's core. Earth Planet Sci Lett 287:77–85

Frost DJ, Liebske C, Langenhorst F, McCammon CA, Tronnes RG, Rubie DC (2004) Experimental evidence for the existence of iron-rich metal in the Earth's lower mantle. Nature 428:409–412

Gao L, Chen B, Wang J, Alp EE, Zhao J, Lerche M et al (2008) Pressure-induced magnetic transition and sound velocities of Fe_3C: implications for carbon in the Earth's inner core. Geophys Res Lett 35:L17306

Garcia RF, Khan A, Drilleau M, Margerin L, Kawamura T, Sun D et al (2019) Lunar seismology: an update on interior structure models. Space Sci Rev 215:50

Garnero EJ, McNamara AK, Shim S-H (2016) Continent-sized anomalous zones with low seismic velocity at the base of Earth's mantle. Nat Geosci 9:481–489

Geiss, J., Gloeckler, G. (1998) Abundances of deuterium and helium-3 in the protosolar cloud. In: Primordial nuclei and their galactic evolution, pp 239–250

Georg RB, Halliday AN, Schauble EA, Reynolds BC (2007) Silicon in the Earth's core. Nature 447:1102–1106

Gessmann CK, Rubie DC (2000) The origin of the depletions of V, Cr and Mn in the mantles of the Earth and Moon. Earth Planet Sci Lett 184:95–107

Gessmann C, Wood B, Rubie D, Kilburn M (2001) Solubility of silicon in liquid metal at high pressure: implications for the composition of the Earth's core. Earth Planet Sci Lett 184:367–376

Giardini D, Lognonné P, Banerdt WB, Pike WT, Christensen U, Ceylan S et al (2020) The seismicity of Mars. Nat Geosci 13:205–212

Grady MM, Wright IP (2003) Elemental and isotopic abundances of carbon and nitrogen in meteorites. Space Sci Rev 106:231–248

Grady MM, Wright I, Pillinger C (1997) Carbon in howardite, eucrite and diogenite basaltic achondrites. Meteorit Planet Sci 32:863–868

Graham DW (2002) Noble gas isotope geochemistry of mid-ocean ridge and ocean island basalts: characterization of mantle source reservoirs. Rev Mineral Geochem 47:247–317

Gray C, Compston W (1974) Excess ^{26}Mg in the Allende meteorite. Nature 251:495–497

Greenberg R, Wacker JF, Hartmann WK, Chapman CR (1978) Planetesimals to planets: numerical simulation of collisional evolution. Icarus 35:1–26

Halliday AN (2004) Mixing, volatile loss and compositional change during impact-driven accretion of the Earth. Nature 427:505–509

Halliday AN (2008) A young Moon-forming giant impact at 70–110 million years accompanied by late-stage mixing, core formation and degassing of the Earth. Philos Trans R Soc A Math Phys Eng Sci 366:4163–4181

Halliday A, Wänke H, Birck J-L, Clayton R (2001) The accretion, composition and early differentiation of Mars. Space Sci Rev 96:197–230

Halliday A, Stirling C, Freedman P, Oberli F, Reynolds B, Georg B (2009) High precision isotope ratio measurements using Multiple Collector Inductively Coupled Plasma Mass Spectrometry. In: Encyclopedia of mass spectrometry

Hallis LJ (2017) D/H ratios of the inner Solar System. Philos Trans R Soc A Math Phys Eng Sci 375:20150390

Hansen BM (2009) Formation of the terrestrial planets from a narrow annulus. Astrophys J 703:1131

Harper CL Jr, Jacobsen SB (1996) Evidence for ^{182}Hf in the early Solar System and constraints on the timescale of terrestrial accretion and core formation. Geochim Cosmochim Acta 60:1131–1153

Hasegawa M, Hirose K, Oka K, Ohishi Y (2021) Liquidus phase relations and solid–liquid partitioning in the Fe–Si–C system under core pressures. Geophys Res Lett 48:092681

Hauck SA, Margot J-L, Solomon SC, Phillips RJ, Johnson CL, Lemoine FG et al (2013) The curious case of Mercury's internal structure. J Geophys Res Planets 118:1204–1220

Hin RC, Schmidt MW, Bourdon B (2012) Experimental evidence for the absence of iron isotope fractionation between metal and silicate liquids at 1 GPa and 1250–1300 °C and its cosmochemical consequences. Geochim Cosmochim Acta 93:164–181

Hin RC, Fitoussi C, Schmidt MW, Bourdon B (2014) Experimental determination of the Si isotope fractionation factor between liquid metal and liquid silicate. Earth Planet Sci Lett 387:55–66

Hirose K, Morard G, Sinmyo R, Umemoto K, Hernlund J, Helffrich G, Labrosse S (2017) Crystallization of silicon dioxide and compositional evolution of the Earth's core. Nature 543:99–102

Hirose K, Tagawa S, Kuwayama Y, Sinmyo R, Morard G, Ohishi Y, Genda H (2019) Hydrogen limits carbon in liquid iron. Geophys Res Lett 46:5190–5197

Holzheid A, Palme H (2007) The formation of eucrites: constraints from metal-silicate partition coefficients. Meteorit Planet Sci 42:1817–1829

Honda M, McDougall I, Patterson DB, Doulgeris A, Clague DA (1991) Possible solar noble-gas component in Hawaiian basalts. Nature 349:149–151

Horita J, Polyakov VB (2015) Carbon-bearing iron phases and the carbon isotope composition of the deep Earth. Proc Natl Acad Sci 112:31–36

Huang H, Fei Y, Cai L, Jing F, Hu X, Xie H et al (2011) Evidence for an oxygen-depleted liquid outer core of the Earth. Nature 479:513–516

Huang H, Leng C, Wang Q, Young G, Liu X, Wu Y et al (2019) Equation of state for shocked Fe–8.6 wt% Si up to 240 GPa and 4,670 K. J Geophys Res Solid Earth 124:8300–8312

Hublet G, Debaille V, Wimpenny J, Yin Q-Z (2017) Differentiation and magmatic activity in Vesta evidenced by ^{26}Al-^{26}Mg dating in eucrites and diogenites. Geochim Cosmochim Acta 218:73–97

Hughes AL, Armitage PJ (2012) Global variation of the dust-to-gas ratio in evolving protoplanetary discs. Mon Not R Astron Soc 423:389–405

Ichikawa H, Tsuchiya T (2020) Ab Initio thermoelasticity of liquid iron–nickel–light element alloys. Minerals 10:59–69

Ichikawa H, Tsuchiya T, Tange Y (2014) The P-V-T equation of state and thermodynamic properties of liquid iron. J Geophys Res Solid Earth 119:240–252

Ida S, Lin D (2008) Toward a deterministic model of planetary formation. V: Accumulation near the ice line and super-Earths. Astrophys J 685:584

Ida S, Makino J (1993) Scattering of planetesimals by a protoplanet: slowing down of runaway growth. Icarus 106:210–227

Ida S, Guillot T, Morbidelli A (2016) The radial dependence of pebble accretion rates: a source of diversity in planetary systems-I: Analytical formulation. Astron Astrophys 591:72

Ikuta D, Ohtani E, Sano-Furukawa A, Shibazaki Y, Terasaki H, Yuan L, Hattori T (2019) Interstitial hydrogen atoms in face-centered cubic iron in the Earth's core. Sci Rep 9:7108

Iwasaki K, Emori H, Nakazawa K, Tanaka H (2002) Orbital stability of a protoplanet system under a drag force proportional to the random velocity. Publ Astron Soc Jpn 54:471–479

Jacobsen SB (2005) The Hf-W isotopic system and the origin of the Earth and Moon. Annu Rev Earth Planet Sci 33:531–570

Jacobsen SB, Ranen MC, Petaev MI, Remo JL, O'Connell RJ, Sasselov DD (2008) Isotopes as clues to the origin and earliest differentiation history of the Earth. Philos Trans R Soc A Math Phys Eng Sci 366:4129–4162

Jacobson SA, Morbidelli A, Raymond SN, O'Brien DP, Walsh KJ, Rubie DC (2014) Highly siderophile elements in Earth's mantle as a clock for the Moon-forming impact. Nature 508:84–87

Javoy M, Kaminski E, Guyot F, Andrault D, Sanloup C, Moreira M et al (2010) The chemical composition of the Earth: enstatite chondrite models. Earth Planet Sci Lett 293:259–268

Johansen A, Lacerda P (2010) Prograde rotation of protoplanets by accretion of pebbles in a gaseous environment. Mon Not R Astron Soc 404:475–485

Johansen A, Youdin A, Klahr H (2009) Zonal flows and long-lived axisymmetric pressure bumps in magnetorotational turbulence. Astrophys J 697:1269

Kadik A, Kurovskaya N, Ignat'ev YA, Kononkova N, Koltashev V, Plotnichenko V (2011) Influence of oxygen fugacity on the solubility of nitrogen, carbon, and hydrogen in FeO–Na_2O–SiO_2–Al_2O_3 melts in equilibrium with metallic iron at 1.5 GPa and 1400 °C. Geochem Int 49:429–438

Kagan Y, Lyubutin IS (1988) Steelmaking data sourcebook. Gordon and Breach Science Publications, New York

Kamada S, Ohtani E, Terasaki H, Sakai T, Miyahara M, Ohishi Y, Hirao N (2012) Melting relationships in the Fe–Fe_3S system up to the outer core conditions. Earth Planet Sci Lett 359:26–33

Kantor AP, Kantor IY, Kurnosov AV, Kuznetsov AY, Dubrovinskaia NA, Krisch M et al (2007) Sound wave velocities of fcc Fe–Ni alloy at high pressure and temperature by mean of inelastic X-ray scattering. Phys Earth Planet Inter 164:83–89

Kawazoe T, Ohtani E (2006) Reaction between liquid iron and (Mg, Fe)SiO_3-perovskite and solubilities of Si and O in molten iron at 27 GPa. Phys Chem Miner 33:227–234

Kennett BL, Engdahl E, Buland R (1995) Constraints on seismic velocities in the Earth from traveltimes. Geophys J Int 122:108–124

Khan A, Connolly J (2008) Constraining the composition and thermal state of Mars from inversion of geophysical data. J Geophys Res Planets 113:E07003

Khan A, Liebske C, Rozel A, Rivoldini A, Nimmo F, Connolly JAD et al (2018) A geophysical perspective on the bulk composition of Mars. J Geophys Res Planets 123:575–611

Kiefer WS, Mittlefehldt DW (2017) Differentiation of asteroid 4 Vesta: core formation by iron rain in a silicate magma ocean. In: Lunar and Planetary Science Conference, p 20170001346. The Woodlands

Kim T, Ko B, Greenberg E, Prakapenka V, Shim SH, Lee Y (2020) Low melting temperature of anhydrous mantle materials at the core-mantle boundary. Geophys Res Lett 47:E89345

Kleine T, Walker RJ (2017) Tungsten isotopes in planets. Annu Rev Earth Planet Sci 45:389–417

Kleine T, Touboul M, Bourdon B, Nimmo F, Mezger K, Palme H et al (2009) Hf–W chronology of the accretion and early evolution of asteroids and terrestrial planets. Geochim Cosmochim Acta 73:5150–5188

Knibbe JS, Rivoldini A, Luginbuhl SM, Namur O, Charlier B, Mezouar M et al (2021) Mercury's interior structure constrained by density and P-wave velocity measurements of liquid Fe–Si–C alloys. J Geophys Res Planets 126:E006651

Kokubo E, Ida S (1995) Orbital evolution of protoplanets embedded in a swarm of planetesimals. Icarus 114:247–257

Kokubo E, Ida S (1996) On runaway growth of planetesimals. Icarus 123:180–191

Komabayashi T (2014) Thermodynamics of melting relations in the system Fe–FeO at high pressure: implications for oxygen in the Earth's core. J Geophys Res Solid Earth 119:4164–4177

Komabayashi T (2021) Phase relations of Earth's core-forming materials. Curr Comput-Aided Drug Des 11:581–632

Kretke KA, Lin D (2007) Grain retention and formation of planetesimals near the snow line in MRI-driven turbulent protoplanetary disks. Astrophys J Lett 664:L55

Krijt S, Ormel CW, Dominik C, Tielens AG (2016) A panoptic model for planetesimal formation and pebble delivery. Astron Astrophys 586:A20

Kuramoto K, Matsui T (1996) Partitioning of H and C between the mantle and core during the core formation in the Earth: its implications for the atmospheric evolution and redox state of early mantle. J Geophys Res Planets 101:14909–14932

Kuwahara H, Itoh S, Nakada R, Irifune T (2019) The effects of carbon concentration and silicate composition on the metal-silicate partitioning of carbon in a shallow magma ocean. Geophys Res Lett 46:9422–9429

Labidi J, Cartigny P, Moreira M (2013) Non-chondritic sulphur isotope composition of the terrestrial mantle. Nature 501:208–211

Labidi J, Shahar A, Le Losq C, Hillgren VJ, Mysen BO, Farquhar J (2016) Experimentally determined sulfur isotope fractionation between metal and silicate and implications for planetary differentiation. Geochim Cosmochim Acta 175:181–194

Lai X, Zhu F, Liu Y, Bi W, Zhao J, Alp EE et al (2020) Elastic and magnetic properties of Fe_3P up to core pressures: phosphorus in the Earth's core. Earth Planet Sci Lett 531:115974

Lambrechts M, Johansen A (2012) Rapid growth of gas-giant cores by pebble accretion. Astron Astrophys 544:A32

Lammer H, Brasser R, Johansen A, Scherf M, Leitzinger M (2020a) Formation of Venus, Earth and Mars: constrained by Isotopes. Space Sci Rev 217:7

Lammer H, Scherf M, Kurokawa H, Ueno Y, Burger C, Maindl T et al (2020b) Loss and fractionation of noble gas isotopes and moderately volatile elements from planetary embryos and early Venus Earth and Mars. Space Sci Rev 216:74

Larsen K, Wielandt D, Schiller M, Krot A, Bizzarro M (2020) Episodic formation of refractory inclusions in the Solar System and their presolar heritage. Earth Planet Sci Lett 535:116088

Levison HF, Thommes E, Duncan MJ (2010) Modeling the formation of giant planet cores. I. Evaluating key processes. Astron J 139:1297–1314

Li J, Agee CB (1996) Geochemistry of mantle–core differentiation at high pressure. Nature 381:686–689

Li J, Agee C (2001) The effect of pressure, temperature, oxygen fugacity and composition on partitioning of nickel and cobalt between liquid Fe–Ni–S alloy and liquid silicate: implications for the Earth's core formation. Geochim Cosmochim Acta 65:1821–1832

Li J, Fei Y (2014) 3.15-Experimental constraints on core composition. In: Heinrich DH, Karl KT (eds) Treatise on geochemistry, 2nd edn. Elsevier, pp 527–557

Li Y, Dasgupta R, Tsuno K (2015) The effects of sulfur, silicon, water, and oxygen fugacity on carbon solubility and partitioning in Fe-rich alloy and silicate melt systems at 3 GPa and 1600 °C: implications for core–mantle differentiation and degassing of magma oceans and reduced planetary mantles. Earth Planet Sci Lett 415:54–66

Li Y, Dasgupta R, Tsuno K, Monteleone B, Shimizu N (2016a) Carbon and sulfur budget of the silicate Earth explained by accretion of differentiated planetary embryos. Nat Geosci 9:781–785

Li Y, Marty B, Shcheka S, Zimmermann L, Keppler H (2016b) Nitrogen isotope fractionation during terrestrial core-mantle separation. Geochem Perspect Lett 2:138–147

Li Y, Vočadlo L, Brodholt J, Wood I (2016c) Thermoelasticity of Fe_7C_3 under inner core conditions. J Geophys Res Solid Earth 121:5828–5837

Li Y, Vočadlo L, Brodholt JP (2018) The elastic properties of hcp-Fe alloys under the conditions of the Earth's inner core. Earth Planet Sci Lett 493:118–127

Li Y, Vočadlo L, Sun T, Brodholt JP (2020) The Earth's core as a reservoir of water. Nat Geosci 13:453–458

Liebske C, Schmickler B, Terasaki H, Poe BT, Suzuki A, Funakoshi K-I et al (2005) Viscosity of peridotite liquid up to 13 GPa: implications for magma ocean viscosities. Earth Planet Sci Lett 240:589–604

Lin DN, Papaloizou J (1986) On the tidal interaction between protoplanets and the protoplanetary disk. III—orbital migration of protoplanets. Astrophys J 309:846–857

Lin J-F, Sturhahn W, Zhao J, Shen G, Mao H-K, Hemley RJ (2005) Sound velocities of hot dense iron: Birch's law revisited. Science 308:1892–1894

Lissauer JJ (1987) Timescales for planetary accretion and the structure of the protoplanetary disk. Icarus 69:249–265

Litasov KD, Shatskiy AF (2016) Composition of the Earth's core: a review. Russ Geol Geophys 57:22–46

Litasov KD, Shatskiy A, Ponomarev DS, Gavryushkin PN (2017) Equations of state of iron nitrides ε-Fe_3N_x and γ-Fe_4N_y to 30 GPa and 1200 K and implication for nitrogen in the Earth's core. J Geophys Res Solid Earth 122:3574–3584

Liu J, Lin J-F, Alatas A, Bi W (2014) Sound velocities of bcc-Fe and $Fe_{0.85}Si_{0.15}$ alloy at high pressure and temperature. Phys Earth Planet Inter 233:24–32

Liu J, Lin JF, Alatas A, Hu MY, Zhao J, Dubrovinsky L (2016a) Seismic parameters of hcp-Fe alloyed with Ni and Si in the Earth's inner core. J Geophys Res Solid Earth 121:610–623

Liu J, Lin JF, Prakapenka VB, Prescher C, Yoshino T (2016b) Phase relations of Fe_3C and Fe_7C_3 up to 185 GPa and 5200 K: implication for the stability of iron carbide in the Earth's core. Geophys Res Lett 43(12):415–444

Liu J, Dauphas N, Roskosz M, Hu MY, Yang H, Bi W et al (2017) Iron isotopic fractionation between silicate mantle and metallic core at high pressure. Nat Commun 8:14377

Lodders K, Fegley B (1997) An oxygen isotope model for the composition of Mars. Icarus 126:373–394

Lorand J-P, Luguet A, Alard O (2013) Platinum-group element systematics and petrogenetic processing of the continental upper mantle: a review. Lithos 164:2–21

Lord OT, Walter MJ, Dasgupta R, Walker D, Clark SM (2009) Melting in the Fe–C system to 70 GPa. Earth Planet Sci Lett 284:157–167

Lord OT, Wann ET, Hunt SA, Walker AM, Santangeli J, Walter MJ et al (2014) The NiSi melting curve to 70 GPa. Phys Earth Planet Inter 233:13–23

Lyra W, Johansen A, Klahr H, Piskunov N (2008) Embryos grown in the dead zone-Assembling the first protoplanetary cores in low mass self-gravitating circumstellar disks of gas and solids. Astron Astrophys 491:L41–L44

Malavergne V, Toplis MJ, Berthet S, Jones J (2010) Highly reducing conditions during core formation on Mercury: implications for internal structure and the origin of a magnetic field. Icarus 206:199–209

Malavergne V, Bureau H, Raepsaet C, Gaillard F, Poncet M, Surblé S et al (2019) Experimental constraints on the fate of H and C during planetary core-mantle differentiation. Implications for the Earth. Icarus 321:473–485

Mao Z, Lin JF, Liu J, Alatas A, Gao L, Zhao J, Mao HK (2012) Sound velocities of Fe and Fe–Si alloy in the Earth's core. Proc Natl Acad Sci 109:10239–10244

Margot JL, Peale SJ, Solomon SC, Hauck SA, Ghigo FD, Jurgens RF et al (2012) Mercury's moment of inertia from spin and gravity data. J Geophys Res Planets 117:E00L09

Margot J-L, Hauck SA II, Mazarico E, Padovan S, Peale SJ (2018) Mercury's internal structure. Cambridge University Press, Cambridge

Marty B (2012) The origins and concentrations of water, carbon, nitrogen and noble gases on Earth. Earth Planet Sci Lett 313–314:56–66

Mashino I, Miozzi F, Hirose K, Morard G, Sinmyo R (2019) Melting experiments on the Fe–C binary system up to 255 GPa: constraints on the carbon content in the Earth's core. Earth Planet Sci Lett 515:135–144

Masset F, Snellgrove M (2001) Reversing type II migration: resonance trapping of a lighter giant protoplanet. Mon Not R Astron Soc 320:L55–L59

Masters G, Gubbins D (2003) On the resolution of density within the Earth. Phys Earth Planet Inter 140:159–167

Matsuda J, Sudo M, Ozima M, Ito K, Ohtaka O, Ito E (1993) Noble gas partitioning between metal and silicate under high pressures. Science 259:788–790

Mavrogenes JA, O'Neill HSC (1999) The relative effects of pressure, temperature and oxygen fugacity on the solubility of sulfide in mafic magmas. Geochim Cosmochim Acta 63:1173–1180

McCord TB, Adams JB, Johnson TV (1970) Asteroid Vesta: spectral reflectivity and compositional implications. Science 168:1445–1447

McCubbin FM, Barnes JJ (2019) Origin and abundances of H_2O in the terrestrial planets, Moon, and asteroids. Earth Planet Sci Lett 526:115771

McCubbin FM, Riner MA, Vander Kaaden KE, Burkemper LK (2012) Is Mercury a volatile-rich planet? Geophys Res Lett 39:L09202

McDonough WF (2001) The composition of the Earth. Academic Press

McDonough W (2014) 3.16-Compositional model for the Earth's core. In: Heinrich DH, Karl KT (eds) Treatise on geochemistry, 2edn. Elsevier, pp 559–577

McDonough WF, Sun S (1995) The composition of the Earth. Chem Geol 120:223–253

Mezger K, Schönbächler M, Bouvier A (2020) Accretion of the Earth—missing components? Space Sci Rev 216:27

Miozzi F, Morard G, Antonangeli D, Baron MA, Boccato S, Pakhomova A et al (2020) Eutectic melting of Fe-3 at% Si-4 at% C up to 200 GPa and implications for the Earth's core. Earth Planet Sci Lett 544:116382

Morard G, Katsura T (2010) Pressure–temperature cartography of Fe–S–Si immiscible system. Geochim Cosmochim Acta 74:3659–3667

Morard G, Andrault D, Guignot N, Sanloup C, Mezouar M, Petitgirard S, Fiquet G (2008) In situ determination of Fe–Fe_3S phase diagram and liquid structural properties up to 65 GPa. Earth Planet Sci Lett 272:620–626

Morard G, Andrault D, Guignot N, Siebert J, Garbarino G, Antonangeli D (2011) Melting of Fe–Ni–Si and Fe–Ni–S alloys at megabar pressures: implications for the core–mantle boundary temperature. Phys Chem Miner 38:767–776

Morard G, Siebert J, Andrault D, Guignot N, Garbarino G, Guyot F, Antonangeli D (2013) The Earth's core composition from high pressure density measurements of liquid iron alloys. Earth Planet Sci Lett 373:169–178

Morard G, Andrault D, Antonangeli D, Nakajima Y, Auzende AL, Boulard E et al (2017) Fe–FeO and Fe–Fe_3C melting relations at Earth's core–mantle boundary conditions: implications for a volatile-rich or oxygen-rich core. Earth Planet Sci Lett 473:94–103

Morbidelli A, Raymond SN (2016) Challenges in planet formation. J Geophys Res Planets 121:1962–1980

Morgan JW, Anders E (1979) Chemical composition of Mars. Geochim Cosmochim Acta 43:1601–1610

Mori Y, Ozawa H, Hirose K, Sinmyo R, Tateno S, Morard G, Ohishi Y (2017) Melting experiments on Fe–Fe_3S system to 254 GPa. Earth Planet Sci Lett 464:135–141

Mysen BO (2003) Physics and chemistry of silicate glasses and melts. Eur J Mineral 15:781–802

Mysen BO, Virgo D, Seifert FA (1982) The structure of silicate melts: implications for chemical and physical properties of natural magma. Rev Geophys 20:353–383

Namur O, Charlier B, Holtz F, Cartier C, McCammon C (2016) Sulfur solubility in reduced mafic silicate melts: implications for the speciation and distribution of sulfur on Mercury. Earth Planet Sci Lett 448:102–114

Neumann W, Breuer D, Spohn T (2014) Differentiation of Vesta: implications for a shallow magma ocean. Earth Planet Sci Lett 395:267–280

Nimmo F, Kleine T (2015) Early differentiation and core formation: processes and timescales. In: The early Earth: accretion and differentiation, pp 83–102

Nishida K, Terasaki H, Ohtani E, Suzuki A (2008) The effect of sulfur content on density of the liquid Fe–S at high pressure. Phys Chem Miner 35:417–423

Nittler LR, Starr RD, Weider SZ, McCoy TJ, Boynton WV, Ebel DS et al (2011) The major-element composition of Mercury's

surface from MESSENGER X-ray spectrometry. Science 333:1847–1850
Ohtani E, Mibe K, Sakamaki T, Kamada S, Takahashi S, Fukui H et al (2015) Sound velocity measurement by inelastic X-ray scattering at high pressure and temperature by resistive heating diamond anvil cell. Russ Geol Geophys 56:190–195
Oka K, Hirose K, Tagawa S, Kidokoro Y, Nakajima Y, Kuwayama Y et al (2019) Melting in the Fe-FeO system to 204 GPa: Implications for oxygen in Earth's core. Am Miner 104:1603–1607
Okuchi T (1997) Hydrogen partitioning into molten iron at high pressure: implications for Earth's core. Science 278:1781–1784
Okuzumi S, Tanaka H, Kobayashi H, Wada K (2012) Rapid coagulation of porous dust aggregates outside the snow line: a pathway to successful icy planetesimal formation. Astrophys J 752:106
Ormel C, Klahr H (2010) The effect of gas drag on the growth of protoplanets-analytical expressions for the accretion of small bodies in laminar disks. Astron Astrophys 520:A43
Ozawa H, Hirose K, Tateno S, Sata N, Ohishi Y (2010) Phase transition boundary between B1 and B8 structures of FeO up to 210 GPa. Phys Earth Planet Inter 179:157–163
Ozawa H, Hirose K, Yonemitsu K, Ohishi Y (2016) High-pressure melting experiments on Fe–Si alloys and implications for silicon as a light element in the core. Earth Planet Sci Lett 456:47–54
Palme H, O'Neil H (2014) 3.1-Cosmochemical estimates of mantle composition. In: Heinrich DH, Karl KT (eds) Treatise on geochemistry, 2nd edn. Elsevier, pp 1–39
Palme H, Rammensee W (1981) Tungsten and some other siderophile elements in meteroitic and terrestrial basalts. Lunar Planet Sci 12:796–798
Pigott JS, Ditmer DA, Fischer RA, Reaman DM, Hrubiak R, Meng Y et al (2015) High-pressure, high-temperature equations of state using nanofabricated controlled-geometry Ni/SiO2/Ni double hot-plate samples. Geophys Res Lett 42:10239–10247
Poitrasson F, Halliday AN, Lee D-C, Levasseur S, Teutsch N (2004) Iron isotope differences between Earth, Moon, Mars and Vesta as possible records of contrasted accretion mechanisms. Earth Planet Sci Lett 223:253–266
Polyakov VB (2009) Equilibrium iron isotope fractionation at core-mantle boundary conditions. Science 323:912–914
Pradhan GK, Fiquet G, Siebert J, Auzende A-L, Morard G, Antonangeli D, Garbarino G (2015) Melting of MORB at core–mantle boundary. Earth Planet Sci Lett 431:247–255
Prescher C, Dubrovinsky L, Bykova E, Kupenko I, Glazyrin K, Kantor A et al (2015) High poisson's ratio of Earth's inner core explained by carbon alloying. Nat Geosci 8:220–223
Pringle EA, Savage PS, Badro J, Barrat J-A, Moynier F (2013) Redox state during core formation on asteroid 4-Vesta. Earth Planet Sci Lett 373:75–82
Ricard Y, Šrámek O, Dubuffet F (2009) A multi-phase model of runaway core–mantle segregation in planetary embryos. Earth Planet Sci Lett 284:144–150
Ricolleau A, Fei Y, Corgne A, Siebert J, Badro J (2011) Oxygen and silicon contents of Earth's core from high pressure metal–silicate partitioning experiments. Earth Planet Sci Lett 310:409–421
Righter K, Chabot NL (2011) Moderately and slightly siderophile element constraints on the depth and extent of melting in early Mars. Meteorit Planet Sci 46:157–176
Righter K, Ghiorso MS (2012) Redox systematics of a magma ocean with variable pressure-temperature gradients and composition. Proc Natl Acad Sci 109:11955–11960
Righter K, Shearer C (2003) Magmatic fractionation of Hf and W: constraints on the timing of core formation and differentiation in the Moon and Mars. Geochim Cosmochim Acta 67:2497–2507
Righter K, Drake M, Yaxley G (1997) Prediction of siderophile element metal-silicate partition coefficients to 20 GPa and 2800 °C: the effects of pressure, temperature, oxygen fugacity, and silicate and metallic melt compositions. Phys Earth Planet Inter 100:115–134
Righter K, King C, Danielson L, Pando K, Lee C (2011) Experimental determination of the metal/silicate partition coefficient of Germanium: implications for core and mantle differentiation. Earth Planet Sci Lett 304:379–388
Righter K, Go B, Pando K, Danielson L, Ross D, Rahman Z, Keller L (2017) Phase equilibria of a low S and C lunar core: implications for an early lunar dynamo and physical state of the current core. Earth Planet Sci Lett 463:323–332
Ringwood AE (1979) Homogeneous accretion revisited. In: Ringwood AE (ed) Origin of the Earth and Moon. Springer, New York, pp 122–134
Rose-Weston L, Brenan JM, Fei Y, Secco RA, Frost DJ (2009) Effect of pressure, temperature, and oxygen fugacity on the metal-silicate partitioning of Te, Se, and S: implications for earth differentiation. Geochim Cosmochim Acta 73:4598–4615
Roskosz M, Bouhifd MA, Jephcoat AP, Marty B, Mysen BO (2013) Nitrogen solubility in molten metal and silicate at high pressure and temperature. Geochim Cosmochim Acta 121:15–28
Rubie DC, Jacobson SA (2016) Mechanisms and geochemical models of core formation. Deep Earth Phys Chem Lower Mantle Core 217:181–190
Rubie DC, Melosh HJ, Reid JE, Liebske C, Righter K (2003) Mechanisms of metal–silicate equilibration in the terrestrial magma ocean. Earth Planet Sci Lett 205:239–255
Rubie DC, Gessmann CK, Frost DJ (2004) Partitioning of oxygen during core formation on the Earth and Mars. Nature 429:58–61
Rubie DC, Frost DJ, Mann U, Asahara Y, Nimmo F, Tsuno K et al (2011) Heterogeneous accretion, composition and core–mantle differentiation of the Earth. Earth Planet Sci Lett 301:31–42
Rubie DC, Jacobson SA, Morbidelli A, O'Brien DP, Young ED, de Vries J et al (2015) Accretion and differentiation of the terrestrial planets with implications for the compositions of early-formed Solar System bodies and accretion of water. Icarus 248:89–108
Russell C, Raymond C, Coradini A, McSween H, Zuber MT, Nathues A et al (2012) Dawn at Vesta: testing the protoplanetary paradigm. Science 336:684–686
Sanloup C, Jambon A, Gillet P (1999) A simple chondritic model of Mars. Phys Earth Planet Inter 112:43–54
Sanloup C, Van Westrenen W, Dasgupta R, Maynard-Casely H, Perrillat J-P (2011) Compressibility change in iron-rich melt and implications for core formation models. Earth Planet Sci Lett 306:118–122
Sata N, Hirose K, Shen G, Nakajima Y, Ohishi Y, Hirao N (2010) Compression of FeSi, Fe_3C, $Fe_{0.95}O$, and FeS under the core pressures and implication for light element in the Earth's core. J Geophys Res Solid Earth 115:9204
Satish-Kumar M, So H, Yoshino T, Kato M, Hiroi Y (2011) Experimental determination of carbon isotope fractionation between iron carbide melt and carbon: ^{12}C-enriched carbon in the Earth's core? Earth Planet Sci Lett 310:340–348
Schiller M, Bizzarro M, Fernandes VA (2018) Isotopic evolution of the protoplanetary disk and the building blocks of Earth and the Moon. Nature 555:507–510
Scott ER, Greenwood RC, Franchi IA, Sanders IS (2009) Oxygen isotopic constraints on the origin and parent bodies of eucrites, diogenites, and howardites. Geochim Cosmochim Acta 73:5835–5853
Shahar A, Schauble EA, Caracas R, Gleason AE, Reagan MM, Xiao Y et al (2016) Pressure-dependent isotopic composition of iron alloys. Science 352:580–582

Shi CY, Zhang L, Yang W, Liu Y, Wang J, Meng Y et al (2013) Formation of an interconnected network of iron melt at Earth's lower mantle conditions. Nat Geosci 6:971–975

Shibazaki Y, Ohtani E, Terasaki H, Suzuki A, Funakoshi K-I (2009) Hydrogen partitioning between iron and ringwoodite: implications for water transport into the Martian core. Earth Planet Sci Lett 287:463–470

Siebert J, Corgne A, Ryerson FJ (2011) Systematics of metal–silicate partitioning for many siderophile elements applied to Earth's core formation. Geochim Cosmochim Acta 75:1451–1489

Siebert J, Badro J, Antonangeli D, Ryerson FJ (2012) Metal–silicate partitioning of Ni and Co in a deep magma ocean. Earth Planet Sci Lett 321–322:189–197

Siebert J, Badro J, Antonangeli D, Ryerson FJ (2013) Terrestrial accretion under oxidizing conditions. Science 339:1194–1197

Simon JB, Armitage PJ (2014) Efficiency of particle trapping in the outer regions of protoplanetary disks. Astrophys J 784:15

Smith DE, Zuber MT, Phillips RJ, Solomon SC, Hauck SA, Lemoine FG et al (2012) Gravity field and internal structure of Mercury from MESSENGER. Science 336:214–217

Sossi PA, Nebel O, Anand M, Poitrasson F (2016) On the iron isotope composition of Mars and volatile depletion in the terrestrial planets. Earth Planet Sci Lett 449:360–371

Speelmanns IM, Schmidt MW, Liebske C (2019) The almost lithophile character of nitrogen during core formation. Earth Planet Sci Lett 510:186–197

Šrámek O, Ricard Y, Dubuffet F (2010) A multiphase model of core formation. Geophys J Int 181:198–220

Stähler SC, Khan A, Banerdt WB, Lognonné P, Giardini D, Ceylan S et al (2021) Seismic detection of the martian core. Science 373:443–448

Steenstra ES, van Westrenen W (2018) A synthesis of geochemical constraints on the inventory of light elements in the core of Mars. Icarus 315:69–78

Steenstra ES, Knibbe JS, Rai N, van Westrenen W (2016) Constraints on core formation in Vesta from metal–silicate partitioning of siderophile elements. Geochim Cosmochim Acta 177:48–61

Steenstra E, Seegers A, Eising J, Tomassen B, Webers F, Berndt J et al (2018) Evidence for a sulfur-undersaturated lunar interior from the solubility of sulfur in lunar melts and sulfide-silicate partitioning of siderophile elements. Geochim Cosmochim Acta 231:130–156

Steenstra ES, Dankers D, Berndt J, Klemme S, Matveev S, van Westrenen W (2019) Significant depletion of volatile elements in the mantle of asteroid Vesta due to core formation. Icarus 317:669–681

Steenstra ES, van Westrenen W (2017) Lunar Magma Ocean, comparison to other planetary Magma Oceans. In: Encyclopedia of Lunar Science, pp 1–6

Stevenson DJ, Scott DR (1991) Mechanics of fluid-rock systems. Annu Rev Fluid Mech 23:305–339

Stevenson DJ (1990) Fluid dynamics of core formation. In: Origin of the Earth, pp 231–249.

Suer T-A, Siebert J, Remusat L, Menguy N, Fiquet G (2017) A sulfur-poor terrestrial core inferred from metal–silicate partitioning experiments. Earth Planet Sci Lett 469:84–97

Tagawa S, Sakamoto N, Hirose K, Yokoo S, Hernlund J, Ohishi Y, Yurimoto H (2021) Experimental evidence for hydrogen incorporation into Earth's core. Nat Commun 12:2588

Takafuji N, Hirose K, Ono S, Xu F, Mitome M, Bando Y (2004) Segregation of core melts by permeable flow in the lower mantle. Earth Planet Sci Lett 224:249–257

Tang H, Dauphas N (2012) Abundance, distribution, and origin of ^{60}Fe in the solar protoplanetary disk. Earth Planet Sci Lett 359:248–263

Tateno S, Hirose K, Sinmyo R, Morard G, Hirao N, Ohishi Y (2018) Melting experiments on Fe–Si–S alloys to core pressures: silicon in the core? Am Miner 103:742–748

Tateyama R, Ohtani E, Terasaki H, Nishida K, Shibazaki Y, Suzuki A, Kikegawa T (2011) Density measurements of liquid Fe–Si alloys at high pressure using the sink–float method. Phys Chem Miner 38:801–807

Taylor GJ (2013) The bulk composition of Mars. Geochemistry 73:401–420

Taylor SR, Jakeš P (1974) Lunar science conference. Pergamon Press, Houston, pp 1287–1305

Taylor FW, Svedhem H, Head JW (2018) Venus: the atmosphere, climate, surface, interior and near-space environment of an Earth-Like planet. Space Sci Rev 214:35

Teng F-Z, Dauphas N, Huang S, Marty B (2013) Iron isotopic systematics of oceanic basalts. Geochim Cosmochim Acta 107:12–26

Terasaki H, Fischer RA (2016) Deep Earth: physics and chemistry of the lower Mantle and Core. American Geophysical Union

Terasaki H, Frost DJ, Rubie DC, Langenhorst F (2005) The effect of oxygen and sulphur on the dihedral angle between Fe–O–S melt and silicate minerals at high pressure: implications for Martian core formation. Earth Planet Sci Lett 232:379–392

Thompson EC, Davis AH, Bi W, Zhao J, Alp EE, Zhang D et al (2018) High-pressure geophysical properties of fcc phase FeH_X. Geochem Geophys Geosyst 19:305–314

Tonks WB, Melosh HJ (1993) Magma ocean formation due to giant impacts. J Geophys Res Planets 98:5319–5333

Toplis MJ, Mizzon H, Monnereau M, Forni O, McSween HY, Mittlefehldt DW et al (2013) Chondritic models of 4 Vesta: implications for geochemical and geophysical properties. Meteorit Planet Sci 48:2300–2315

Touboul M, Sprung P, Aciego SM, Bourdon B, Kleine T (2015) Hf–W chronology of the eucrite parent body. Geochim Cosmochim Acta 156:106–121

Trønnes RG, Baron MA, Eigenmann KR, Guren MG, Heyn BH, Løken A, Mohn CE (2019) Core formation, mantle differentiation and core-mantle interaction within Earth and the terrestrial planets. Tectonophysics 760:165–198

Tsuno K, Frost DJ, Rubie DC (2011) The effects of nickel and sulphur on the core–mantle partitioning of oxygen in Earth and Mars. Phys Earth Planet Inter 185:1–12

Tsuno K, Frost DJ, Rubie DC (2013) Simultaneous partitioning of silicon and oxygen into the Earth's core during early Earth differentiation. Geophys Res Lett 40:66–71

Tsuno K, Grewal DS, Dasgupta R (2018) Core-mantle fractionation of carbon in Earth and Mars: the effects of sulfur. Geochim Cosmochim Acta 238:477–495

Vander Kaaden KE, McCubbin FM, Turner AA, Ross DK (2019) Constraints on the abundances of carbon and silicon in Mercury's core from experiments in the Fe–Si–C system. J Geophys Res Planets 125:006239

Vočadlo L, Dobson DP, Wood IG (2009) Ab initio calculations of the elasticity of hcp-Fe as a function of temperature at inner-core pressure. Earth Planet Sci Lett 288:534–538

Wada K, Tanaka H, Suyama T, Kimura H, Yamamoto T (2009) Collisional growth conditions for dust aggregates. Astrophys J 702:1490

Wada K, Tanaka H, Okuzumi S, Kobayashi H, Suyama T, Kimura H, Yamamoto T (2013) Growth efficiency of dust aggregates through collisions with high mass ratios. Astron Astrophys 559:A62

Wade J, Wood BJ (2005) Core formation and the oxidation state of the Earth. Earth Planet Sci Lett 236:78–95

Walsh KJ, Levison HF (2016) Terrestrial planet formation from an annulus. Astron J 152:68

Walsh KJ, Morbidelli A, Raymond SN, O'Brien DP, Mandell AM (2011) A low mass for Mars from Jupiter's early gas-driven migration. Nature 475:206–209

Walte N, Heidelbach F, Miyajima N, Frost D (2007) Texture development and TEM analysis of deformed $CaIrO_3$: implications for the D″ layer at the core-mantle boundary. Geophys Res Lett 34:L08306

Wang H, Weiss BP, Bai X-N, Downey BG, Wang J, Wang J et al (2017) Lifetime of the solar nebula constrained by meteorite paleomagnetism. Science 355:623–627

Wänke H, Dreibus G (1988) Chemical composition and accretion history of terrestrial planets. Philos Trans R Soc A Math Phys Eng Sci 325:545–557

Warren PH (2011) Stable-isotopic anomalies and the accretionary assemblage of the Earth and Mars: a subordinate role for carbonaceous chondrites. Earth Planet Sci Lett 311:93–100

Waseda Y, Shiraishi Y, Toguri JM (1980) The structure of the molten $FeO–Fe_2O_3–SiO_2$ system by X-ray diffraction. Trans Jpn Inst Met 21:51–62

Weber RC, Lin PY, Garnero EJ, Williams Q, Lognonne P (2011) Seismic detection of the lunar core. Science 331:309–312

Weidenschilling S (1980) Dust to planetesimals: settling and coagulation in the solar nebula. Icarus 44:172–189

Weidenschilling S (1995) Can gravitational instability form planetesimals? Icarus 116:433–435

Wetherill GW (1985) Occurrence of giant impacts during the growth of the terrestrial planets. Science 228:877–879

Wetherill G, Stewart GR (1989) Accumulation of a swarm of small planetesimals. Icarus 77:330–357

Weyer S, Anbar A, Brey G, Munker C, Mezger K, Woodland A (2005) Iron isotope fractionation during planetary differentiation. Earth Planet Sci Lett 240:251–264

Whipple FL (1972) From plasma to planet, p 211

Williams HM, Markowski A, Quitté G, Halliday AN, Teutsch N, Levasseur S (2006) Fe isotope fractionation in iron meteorites: new insights into metal-sulphide segregation and planetary accretion. Earth Planet Sci Lett 250:486–500

Woo JMY, Brasser R, Matsumura S, Mojzsis SJ, Ida S (2018) The curious case of Mars' formation. Astron Astrophys 617:A17

Wood JA, Dickey JS Jr, Marvin UB, Powell B (1970) Lunar anorthosites and a geophysical model of the moon. Geochim Cosmochim Acta Suppl 1:965

Wood BJ, Walter MJ, Wade J (2006) Accretion of the Earth and segregation of its core. Nature 441:825–833

Wood BJ, Li J, Shahar A (2013) Carbon in the core: its influence on the properties of Core and Mantle. Rev Mineral Geochem 75:231–250

Wu J, Desch SJ, Schaefer L, Elkins-Tanton LT, Pahlevan K, Buseck PR (2018) Origin of Earth's water: chondritic inheritance plus nebular ingassing and storage of hydrogen in the core. J Geophys Res Planets 123:2691–2712

Yin Q, Jacobsen S, Yamashita K, Blichert-Toft J, Télouk P, Albarede F (2002) A short timescale for terrestrial planet formation from Hf–W chronometry of meteorites. Nature 418:949–952

Yokoo S, Hirose K, Sinmyo R, Tagawa S (2019) Melting experiments on liquidus phase relations in the Fe–S–O ternary system under core pressures. Geophys Res Lett 46:5137–5145

Yoshioka T, Wiedenbeck M, Shcheka S, Keppler H (2018) Nitrogen solubility in the deep mantle and the origin of Earth's primordial nitrogen budget. Earth Planet Sci Lett 488:134–143

Yoshizaki T, McDonough WF (2020) The composition of Mars. Geochim Cosmochim Acta 273:137–162

Youdin AN, Goodman J (2005) Streaming instabilities in protoplanetary disks. Astrophys J 620:459

Yu G, Jacobsen SB (2011) Fast accretion of the Earth with a late Moon-forming giant impact. Proc Natl Acad Sci 108:17604–17609

Zhang Y, Yin Q (2012) Carbon and other light element contents in the Earth's core based on first-principles molecular dynamics. Proc Natl Acad Sci 109:19579–19583

Zhang Y, Sekine T, He H, Yu Y, Liu F, Zhang M (2014) Shock compression of Fe–Ni–Si system to 280 GPa: implications for the composition of the Earth's outer core. Geophys Res Lett 41:4554–4559

Zhou J, Lin DN, Sun Y (2007) Post-oligarchic evolution of protoplanetary embryos and the stability of planetary systems. Astrophys J 666:423

Zhu F, Lai X, Wang J, Amulele G, Kono Y, Shen G et al (2021) Density of Fe–Ni–C liquids at high pressures and implications for liquid cores of Earth and the Moon. J Geophys Res Solid Earth 126:021089

Ziegler K, Young ED, Schauble EA, Wasson JT (2010) Metal–silicate silicon isotope fractionation in enstatite meteorites and constraints on Earth's core formation. Earth Planet Sci Lett 295:487–496

Zolotov MY, Sprague AL, Hauck SA, Nittler LR, Solomon SC, Weider SZ (2013) The redox state, FeO content, and origin of sulfur-rich magmas on Mercury. J Geophys Res Planets 118:138–146

Zsom A, Ormel CW, Güttler C, Blum J, Dullemond C (2010) The outcome of protoplanetary dust growth: pebbles, boulders, or planetesimals?—II. Introducing the bouncing barrier. Astron Astrophys 513:57

Zube NG, Nimmo F, Fischer RA, Jacobson SA (2019) Constraints on terrestrial planet formation timescales and equilibration processes in the Grand Tack scenario from Hf-W isotopic evolution. Earth Planet Sci Lett 522:210–218

Zuber MT, Smith DE, Phillips RJ, Solomon SC, Neumann GA, Hauck SA et al (2012) Topography of the northern hemisphere of Mercury from MESSENGER laser altimetry. Science 336:217–220